Magnetic resonance imaging of the human locus coeruleus: A systematic review

Authors:

Kathy Y Liu[1]*, Freya Marijatta[2], Dorothea Hämmerer[3,5], Julio Acosta-Cabronero[4], Emrah Düzel[5], Robert J Howard[1]

Affiliations:

[1] Division of Psychiatry, University College London, UK

[2] Division of Psychology and Language Sciences, University College London, UK

[3] Institute of Cognitive Neuroscience, University College London, UK

[4] Wellcome Trust Centre for Neuroimaging, UCL Institute of Neurology, University College London, UK

[5] German Centre for Neurodegenerative Diseases (DZNE), Magdeburg, Germany

*corresponding author. Email address kathy.liu@ucl.ac.uk

Abstract:

The locus coeruleus (LC), the major origin of noradrenergic modulation of the central nervous system, innervates extensive areas throughout the brain and is implicated in a variety of autonomic and cognitive functions. Alterations in the LC-noradrenergic system have been associated with healthy ageing and neuropsychiatric disorders including Parkinson's disease, Alzheimer's disease and depression. The last decade has seen advances in imaging the structure and function of the LC, and this paper systematically reviews the methodology and outcomes of sixty-nine structural and functional MRI studies of the LC in humans. Structural MRI studies consistently showed lower LC signal intensity and volume in clinical groups compared to healthy controls. Within functional studies, the LC was activated by a variety of tasks/stimuli and had functional connectivity to a range of brain regions. However, reported functional LC location coordinates were widely distributed compared to previously published neuroanatomical locations. Methodological and demographic factors potentially contributing to these differences are

discussed, together with recommendations to optimize the reliability and validity of future LC imaging studies.

1. Introduction:

The locus coeruleus (LC) is a cylindrical, hyperpigmented nucleus located in the rostral pontine brainstem. It is the major origin of noradrenergic neurones in the central nervous system. In histological specimens, the average dimensions of the human LC have been measured as 14.5mm in length and 2.5mm in thickness (2mm in the central portion) (Fernandes et al., 2012). Its cylindrical shape is thinner in its central part and diverges laterally in its caudal three-fourths (see Figure 1).

<<Figure 1>>

The LC plays an integral role in the regulation of arousal and autonomic function through connections with widespread areas of the brain and spinal cord (Samuels and Szabadi, 2008a), modulating wakefulness, pupil control, blood pressure and temperature. It also plays a role in anxiogenesis and responses to fear and pain via connections with the amygdala (Samuels and Szabadi, 2008b), and has been implicated in cognitive processes including attention, decision-making and memory through connections with frontal cortex and the hippocampus (Sara, 2009). In humans, LC neuron numbers are believed to gradually decline with increasing age (Mann, 1983) although some reports

1

challenge this view and suggest that LC neuronal death in cognitively normal older adults might indicate a presymptomatic stage of dementia-related physiological decline (Mather and Harley, 2016). Neuromelanin, a dark polymer pigment accumulates inside the noradrenergic neurons of the LC until the age of about 60 years, after which it declines, possibly in association with preferential loss of neurons containing the highest neuromelanin content (Mann and Yates, 1974).

The LC has been the subject of increasing interest within neurology and psychiatry following demonstration of early pathological change in neurodegenerative conditions such as Parkinson's disease (PD) and Alzheimer's disease (AD), conditions that have traditionally been more associated with dysfunction in the dopaminergic and cholinergic systems respectively (Zarow et al., 2003). Early tau pathology in the LC may even precede the hallmark appearance of tau and amyloid pathology in the medial temporal lobe and in cortical regions in AD (Braak et al., 2011) and has been shown to be associated with LC volume loss as the disease progresses (Theofilas et al., 2016). LC neurofibrillary tangles and abnormal tau show an age-MCI-AD continuum, with levels of cytopathology being associated with cognitive impairment (Grudzien et al., 2007). Studies have also implicated LC and noradrenergic system alterations in the pathophysiology of other disorders including depression (Arango et al., 1996; Bernard et al., 2011; Ressler and Nemeroff, 1999), schizophrenia (Lohr and Jeste, 1988; Yamamoto and Hornykiewicz, 2004), addiction (Berridge and Waterhouse, 2003/4) and autism (Mehler and Purpura, 2009).

<<Figure 2>>

The human LC can be visualized using T1-weighted MRI (Sasaki et al., 2008b) (see also Figure 2). Neuromelanin scavenges metals such as iron and copper (Sasaki et al., 2008a), which confers T1-shortening effects resulting in signal hyperintensity on T1-weighted images (Enochs et al., 1997; Trujillo et al., 2016). As neuromelanin is found inside the noradrenergic neurones of the LC and in the dopaminergic neurons of the substantia nigra in humans, these structures can be readily visualized using T1-weighted as well as magnetization transfer (MT) weighted MRI (Nakane et al., 2008; Sasaki et al., 2006).

In addition to neuromelanin-content enhancing T1- or MT-weighted approaches, often referred to as 'neuromelanin-sensitive' imaging, functional MRI techniques have also been used to investigate LC activity and connectivity in healthy and clinical human populations. However, no previous review has summarized the characteristics and findings of structural and functional MRI studies of the LC, and no consensus on recommendations to achieve optimal methodological validity and reliability has been published. Optimal in-vivo imaging of the LC is needed to evaluate its potential as a biomarker in neuropsychiatric conditions such as dementia and to assess the efficacy of future treatments targeting the LC-noradrenergic system.

This paper systematically reviews the studies that have published data on the LC using functional or structural MRI techniques. For neuromelanin-optimized structural MRI

studies, the review includes the range of scanning parameters used and methods employed to localize and measure the LC, and compares measures of signal intensity obtained in healthy and clinical populations. For functional imaging studies, the review describes the methods used to localize the LC and compares the distribution of location coordinates attributed to the LC with published neuropathological location data. The tasks and conditions associated with LC activation are also reported. Finally, a critical summary of the methodological factors that may limit validity are discussed, together with recommendations to optimize the reliability and validity of future LC imaging studies.

2. Method:

2.1 Literature search

Online literature databases (PubMed, PsycINFO, Embase and Web of Science) were searched up to (12th April 2017) using the search terms ("locus coeruleus" OR "locus caeruleus" OR "locus ceruleus") AND magnetic resonance imaging.

2.2 Inclusion/exclusion criteria and screening

Studies were included if they were peer-reviewed papers that reported novel findings on the LC in human subjects of any age, with any or no health condition. Also papers that used terms such as locus coeruleus complex (LCC), nucleus coeruleus or reported on 'a brainstem region tentatively identified as LC' were included for the purposes of the review. Functional MRI studies were included if they reported spatial coordinates (x, y, z) for the LC.

Studies were excluded if they investigated a brainstem region but did not report data specific to the LC, or failed to describe their methods in any detail. Case reports, poster abstracts and dissertations were also excluded.

2.3 Data extraction

Two authors (KL and DH) independently screened papers for inclusion based on their titles and abstracts. Two authors (KL and FM) subsequently extracted data on study characteristics, MRI protocol and outcome measures using a structured form. Where studies only reported the acquired pixel size and slice thickness, these were converted to voxel size. Discrepancies were resolved through discussion among the coauthors.

2.4 Statistical analysis

2.4.1 Structural imaging studies

To measure and compare LC integrity between different clinical groups, neuromelanin-optimized imaging studies have commonly reported the LC contrast ratio (CR, see equation below). Conditions such as AD and PD are hypothesized to be associated with impaired LC integrity, i.e. lower CR values relative to those in healthy controls. To compare the CR obtained for different clinical groups, the weighted means and confidence intervals for each group were calculated and plotted. The weight applied to each value was determined by the number of subjects in each group. Only studies that reported numerical data for the mean or median CR using the following formula were included for the analysis:

$$CR = \frac{(S_{LC} - S_{ref})}{S_{ref}},$$ (Equation 1)

where S_{LC} represents the signal intensity of the LC and S_{ref}, the signal intensity of a reference region. This was the most commonly used formula to calculate CR. Studies that used a different formula to measure the signal from the LC were excluded from the analysis. The CR values from Mather et al. (2017) were also excluded as they originated from and were already reported in Clewett et al. (2016). The mean and not the median CR was used from (Ehrminger et al., 2016), and the average CR was calculated from the middle, rostral and caudal CR values for each participant group from (Shibata et al., 2007).

2.4.2 Functional imaging studies

To compare the distribution of coordinates of activation attributed to the LC in functional MRI studies, we used a bootstrap analysis method described in a previous systematic review (Costafreda et al., 2006) to construct confidence intervals for the weighted mean Montreal Neurological Institute (MNI) location coordinates along each of the spatial axes (x, y, z). The weight applied to each individual peak activation was proportional to the number of subjects in the experiment. Due to the anatomical shape of the LC, which is described as diverging caudally from the midline in its lower three fourths (Fernandes et al., 2012), the studies were divided into four bins along the range of reported z-coordinates before calculating the bootstrap confidence intervals and weighted means of the location coordinates for each bin. To assess the validity of these findings, they were compared to location coordinates previously published by Keren et al. (2009), as this

6

was the only study from the literature search that had published a histologically validated location map of the LC in MNI coordinates. If a study reported more than one LC location using the same method these were all included in the analysis, however only the unsmoothed data from Murphy et al., (2014) and the coordinates obtained using the specialized template (SUIT) from Köhler et al., (2016) were included. Functional studies that reported only Talairach coordinates were included after transforming their location data into MNI space (Lacadie et al., 2008).

<h3>3. Results</h3>

3.1 Identification and characteristics of included studies

Literature searches identified 838 potential studies, 69 of which met inclusion criteria for data extraction (Figure 3, PRISMA flow diagram). Thirty-seven of these employed a cross-sectional design with no comparison group, n=28 were case-control studies, and four studies were randomized controlled trials.

The majority of studies (n=42) involved healthy, non-clinical participants, n=23 studies were in a defined neuropsychiatric population (e.g. MCI/dementia, depression, schizophrenia, post-traumatic stress disorder, generalized anxiety disorder) and three were in other clinical disorders (e.g. migraine, chronic regional pain syndrome, irritable bowel syndrome). In structural MRI studies, the condition most frequently investigated was PD. In functional studies, the cognitive functions most frequently investigated were cognitive control/decision-making and attention. Most studies (n=43) tested younger adults between 18-65 years old (mean age: 29 y.o.), n=23 studies looked at both younger and older adults (mean age: 58 y.o.), and two studies tested children (mean

age: 13 y.o.). The number of years of education was included in 4% of all studies, handedness was reported in 29% of all studies and 51% of all study participants were female.

3.2 Structural MRI assessment of the LC

Table 1 summarizes the characteristics of 28 studies that reported data on the LC using structural MRI. Within these studies, most (n=25) used neuromelanin-optimized T1-weighted MRI, three used standard T1-weighted anatomical scans obtained to aid localization of positron emission tomography (PET), and an additional MRI study also employed diffusion tensor imaging (DTI). Anatomical scans that were acquired as part of fMRI studies to aid co-registration were not included here as they did not provide data specific to the LC.

Most neuromelanin-sensitive approaches developed to date to image the LC differ in MRI acquisition parameters and in their methodology to localize the structure and measure signal properties. The overall differences in LC signal intensity between and within clinical populations investigated in these studies are also summarized below (Table 1)

3.2.1 MRI scanning parameters and co-registration techniques

Table 2 shows the imaging parameters that were reported on the 25 studies that sensitized MRI to neuromelanin content in the LC. The majority (21 studies) used a T1-weighted rapid acquisition with refocused echoes (RARE) pulse sequence, also known

as turbo/fast spin echo (TSE/FSE). Three studies, in contrast, prescribed T1 weighting with inversion recovery (IR) approaches – multi-inversion RARE (Keren et al., 2015) and spectral presaturation inversion recovery (SPIR) (Schwarz, 2012; Schwarz et al., 2016). In addition, two studies employed 2D gradient echo (GRE) sequences with an off-resonance MT pre-saturation pulse (Chen et al., 2014; Langley et al., 2016), and one study used 3D-spoiled, steady-state GRE (GRASS) with MT preparation (Watanabe et al., 2014). Almost all studies were carried out *in vivo* using scanners with a magnetic field strength of either 1.5 Tesla (T) or 3T. Two *ex vivo* studies scanned brainstem specimens (Keren et al., 2015, 2009) of which one prescribed an IR approach using 7T MRI. Notably, however, many studies did not report all the relevant MRI parameters, thus Table 2 is somewhat incomplete.

A common feature in the selected studies is the prescription of higher in-plane resolution than slice thickness, resulting in elongated voxels that match the cylindrical shape of the LC. The reported slice thickness ranged between 2-3 mm, the largest interslice gap reported was 3.5mm (Clewett et al., 2016; Mather et al., 2017). In-plane resolution varied, and voxel size ranged from $0.31x0.36x2.5mm^3$ (Sasaki et al., 2006) to $0.5x0.5x3mm^3$ (Isaias et al., 2016) (see Table 2). The scan duration for *in vivo* studies ranged from 1:53 minutes to obtain one signal average (Clewett et al., 2016; Mather et al., 2017) to 17:12 minutes for 7 averages (Langley et al., 2016). Finally, it is noteworthy that the most common plane of acquisition (used by 11 studies) was oblique-axial perpendicular to the floor of the fourth ventricle.

Eight studies described co-registering MR images to each other or to an anatomical template. The templates used varied and included the International Consortium for Brain Mapping (ICBM) and MNI152 (Ehrminger et al., 2016; Langley et al., 2016), study-wise T1-anatomical images (Castellanos et al., 2015; García-Lorenzo et al., 2013) or the Colin27 template (Castellanos et al., 2015). Images of histologic specimens were also co-registered (Keren et al., 2015) or correlated (Sasaki et al., 2006) with MRI images to validate the source or location of the neuromelanin signal.

3.2.2 Localization of the LC, measurement of signal intensity and LC volume
In most studies, the LC was identified, or segmented manually, and signal intensity was measured within a predefined brainstem area. Three studies employed semi-automated segmentation methods to calculate CR and/or LC volume (Chen et al., 2014; Langley et al., 2016; Sasaki et al., 2010) and one used a fully automated segmentation method to calculate LC volume (Castellanos et al., 2015).

The size of the LC mask varied. Most studies detected the peak intensity within either a 1-2mm^2 circular region or a single voxel, and two studies calculated signal intensity from the average of the 10 brightest interconnected voxels (Ehrminger et al., 2016; García-Lorenzo et al., 2013). In addition, one study compared the signal intensities of the middle, rostral and caudal portions of the LC (Shibata et al., 2007). Notably, however, only 12 (out of 22) studies reported that measurements were carried out blinded to participant status.

All studies, apart from two (Keren et al., 2015, 2009), normalized LC signal intensity to that of a neighbouring reference region – the pons/pontine tegmentum (16 studies), rostral pontomesencephalic area (two studies) and cerebral peduncle (one study). Such studies reported on the contrast ratio (CR), i.e. the outcome measure assessed in the present study, with the great majority using CR as in Eq. 1; however, some differed in the terminology used. The same formulation, for example, was also referred to as magnetisation transfer contrast (MTC) (Langley et al., 2016) or contrast-to-noise ratio (CNR) (Clewett et al., 2016). Additionally, one study calculated CR as SI_{LC}/SI_{ref} (Schwarz, 2012), and two studies calculated CNR as follows: $CNR=(SI_{LC}-SI_{ref})/SD_{ref}$, where SI represents mean signal intensity and SD_{ref} is the standard deviation of the signal in the reference region (Chen et al., 2014; Isaias et al., 2016).

Twelve studies reported the mean CR or CNR, and one presented the data only graphically. Five studies reported the median CR or CNR, and two presented this only graphically.

Only four studies reported on LC volume, which were $8.2mm^3$ and $11.7mm^3$ in Parkinson's disease, and $15.2mm^3$ and $16.7mm^3$ in healthy controls (Castellanos et al., 2015; Schwarz et al., 2016), respectively; and what appears to be between $1.8-8.8mm^3$ (Chen et al., 2014) and $10-30mm^3$ (Langley et al., 2016) on a graphical plot in healthy adults. Based on the mean width (2-2.5mm) and length (14.5mm) of the LC from post-mortem data (Fernandes et al., 2012), one would expect the actual LC volume to be around $50mm^3$ in healthy adults. One study reported the area of the LC to be between

10.8mm^2 in schizophrenia and 11.4mm^2 in healthy controls (Watanabe et al., 2014).

3.2.3 Main findings in healthy and clinical populations

<<Figure 4>>

Figure 4 shows the distribution, weighted means and 95% confidence intervals of mean and median CR values for clinical participant groups in studies that used Eq. 1. Only one study reported numerical CR data in patients with AD (Takahashi et al., 2015), thus a weighted mean and confidence interval could not be constructed for this group. On average, compared to healthy controls, CR was lower in all patient groups (MD, SZ, PD, AD and MCI), but more studies are needed to confirm this observation with a targeted investigation of specific clinical groups. The age ranges of each group were: 18-80 years (HC), 22-83 years (MD), 17-69 years (SZ), 41-85 years (PD), 59-86 years (AD), and 60-87 years (MCI). The HC and PD groups had the highest number of studies so were the only groups to be statistically compared. The difference in CR between the HC and PD groups was significant ($p < 0.05$) after analysis using a nonparametric test (Mann-Whitney U test z= -2.56, p=0.009). However, due to the limited sample size, this result should be viewed cautiously. Overall differences between the other groups were not calculated due to their very small sample sizes.

Findings in healthy adults

In healthy participants, one study found that the CR increased with age until 40-59 years

and then decreased, with no significant difference between men and women (Shibata et al., 2006). In contrast, (Clewett et al., 2016) found that the LC in older adults (mean age 67) had greater CR than that in younger adults (mean age 24), and this was positively associated with measures of cognitive reserve in older adults. Both studies accorded their findings with evidence that LC neuromelanin accrues in an inverted U pattern across the lifespan with peak concentrations occurring at around 60 years (Mann and Yates, 1974; Manaye et al., 1995). It is conceivable, however, that an LC- CR increase in older adults could partly be explained by their concurrent finding of an age-related decrease in the signal intensity of the reference region (pontine tegmentum). The authors also reported a lower CR in women than in men, which is interesting given some evidence of increased risk of AD in females compared to males (Altmann et al., 2014; Andersen et al., 1999).

Findings in Parkinson's disease

Ten studies investigated patients with PD or parkinsonism compared to a healthy control (HC) group. Apart from one study which found no significant difference in the LC between PD and HC, most LC studies reported reduced CR (or CNR) in PD compared to HC (Isaias et al., 2016; Matsuura et al., 2013; Miyoshi et al., 2013; Mukai et al., 2013; Ohtsuka et al., 2014; Sasaki et al., 2006) and reduced LC volume in PD compared to HC (Castellanos et al., 2015). Using the CR, LC-optimized T1-weighted MRI did not distinguish between early and advanced PD (Ohtsuka et al., 2013), though interestingly, the same study found differences between PD and other parkinsonian syndromes such as multiple system atrophy (MSA) (Matsuura et al., 2013; Ohtsuka et al., 2014), and

reduced LC signal intensity in PD with REM-sleep behavior disorder (RBD) compared to PD without RBD (García-Lorenzo et al., 2013). Furthermore, a study that did not include participants with PD also reported reduced CR in RBD compared to HC (Ehrminger et al., 2016).

Findings in Alzheimer's disease (AD) and Mild Cognitive Impairment (MCI)

Two *in vivo* studies investigated patients with AD and MCI and compared them to HC with different findings. (Takahashi et al., 2015) found reduced LC-CR in AD and MCI compared to HC but no difference between the AD and MCI groups. In contrast, (Miyoshi et al., 2013) did not find a significant difference in CR between AD and HC groups.

Findings in Major Depression and Schizophrenia

Four studies investigated patients with diagnoses of Major Depression (MD) and/or Schizophrenia (SZ) compared to HC. SZ studies did not find significant CR alterations relative to controls (Sasaki et al., 2010; Shibata et al., 2008; Watanabe et al., 2014); though notably, CR differences were identified between the substantia nigra and LC (Sasaki et al., 2010; Shibata et al., 2008). Two studies reported significantly reduced CR in MD compared to both HC and SZ (Sasaki et al., 2010; Shibata et al., 2008), and one found reduced CR of the rostral and middle LC in MD patients compared to HC, but this did not correlate with scores on psychiatric rating scales (Shibata et al., 2007).

Taken together, studies to date suggest that some patient populations might have lower CR values in the LC than healthy adults, however, more studies are needed to

strengthen this observation. Differences in CR did not correlate with symptom severity scores in MD and SZ, but it successfully distinguished between PD and other parkinsonian syndromes, and between PD with and without RBD. There is some evidence for age-related changes in CR in healthy adults and possible differences between males and females, however there is no consensus on the precise nature of these differences. Despite data showing healthy subjects with lower LC volumes than expected based on neuroanatomical data, there was a difference in volume between this group and PD patients.

3.3 Functional MRI

Table 3 summarizes the characteristics of 41 studies that reported functional MRI (fMRI) data from the LC. Within these studies, 25 reported event-related BOLD data from the LC and 13 reported on functional connectivity between other brain regions and the LC. Three studies reported both BOLD and functional connectivity data. Nine functional connectivity studies involved resting state data.

3.3.1 Coregistration and other preprocessing methods

Due to the small size of the LC, precise coregistration between functional and structural MRI images is required. This is because the LC can only be visualized in structural images and via coregistration needs to be accurately identified in the functional images. The majority of fMRI studies described performing a coregistration procedure, and only 6 studies did not. Two studies obtained structural T1-TSE neuromelanin-optimized MRI images for coregistration with BOLD images for precise anatomical localisation (Krebs et

al., 2017; Murphy et al., 2014). The imaging data was spatially normalized into Montreal Neurological Institute (MNI) space in most studies but 3 papers transformed their MRI data into Talairach space (Anticevic et al., 2014; Kraus et al., 2013; Lerner et al., 2009). To improve normalization within the brainstem, two studies normalized neuroimaging data to the spatially unbiased infratentorial template (SUIT), a high-resolution atlas template of the human cerebellum and brainstem based on the anatomy of 20 healthy individuals (Bär et al., 2016; Köhler et al., 2016). This method produced different MNI location coordinates for the LC when compared to the normalization process on the same data using the standard ICBM atlas template (Köhler et al., 2016). No study was judged to have adequately reported how the precision of the coregistration method was assessed.

The acquired voxel size reported ranged from 1.2x1.2x1.2mm^3 (Sclocco et al., 2016) to 3.75x3.75x4mm^3 (Xuan et al., 2016) (see Table 3). Where reported, functional images were resampled to 2x2x2mm^3 voxels (7 studies), 1x1x1mm^3 voxels (2 studies) or 3x3x3mm^3 voxels (1 study). The majority of studies (30) subsequently spatially smoothed the images using a Gaussian kernel of a size that varied between 2mm and 8mm full width half maximum (FWHM). Only seven studies described correcting data for both cardiac and respiratory noise signals.

3.3.2 Localization of the LC

Functional MRI studies that used a region-of-interest (ROI) analysis to measure the LC identified the LC ROI using different methods. Previously published coordinates of the

LC were often used to identify the ROI, most commonly derived from Keren et al., (2009) which used ex-vivo neuromelanin-optimized T1-weighted imaging (Hubbard et al., 2011; Kahnt and Tobler, 2013; Laureiro-Martínez et al., 2015; Murphy et al., 2014; Payzan-LeNestour et al., 2013; Schulte et al., 2016), but also from a structural MRI study by Astafiev et al., (2010) (Henckens et al., 2012; Laureiro-Martínez et al., 2015; Morey et al., 2015). Some studies referenced coordinates obtained from previously published functional MRI studies: three studies used data from Liddell et al., 2005, two used coordinates from Sterpenich et al., 2006 (which itself references Liddell et al., 2005), and one study used data from Schmidt et al., (2009) (which itself references Liddell et al., 2005 and Sterpenich et al., 2006). Eight fMRI studies used an exploratory whole-brain analysis approach and defined the LC ROI according to the location of activity contrast between participant conditions.

Where methodology was reported, a LC mask was generated from the average structural scans of the group (Brooks et al., 2017) or was obtained using a different template (e.g. ICBM 152) (Köhler et al., 2016; Sclocco et al., 2016; Xuan et al., 2016) to aid localization of the LC on individual functional scans. One study reported using a subject's anatomical brainstem dataset as a reference brainstem, and manually transformed other participants' functional activations onto this (Kraus et al., 2013).

Five functional connectivity studies used the LC as their seed region. Location coordinates for the seed region were obtained from different sources, including a previous study by Keren et al., (2009) (Kline et al., 2016; Zhang et al., 2016), a previous

study published by the same author (Steuwe et al., 2015), and an anatomical atlas of the human brainstem (Duvornoy's Atlas of the Human Brainstem and Cerebellum by Naidich et al., 2009) (Bär et al., 2016).

3.3.3 Independent variables investigated

The majority of fMRI studies of the LC investigated executive functions, including attention (Mohanty et al., 2008; Murphy et al., 2014; Neufang et al., 2015; Raizada and Poldrack, 2007; Xuan et al., 2016), cognitive or inhibitory control (Köhler et al., 2016; Minzenberg et al., 2008; Schilbach et al., 2011; von der Gablentz et al., 2015) and decision-making (Kahnt and Tobler, 2013; Laureiro-Martínez et al., 2015; Payzan-LeNestour et al., 2013). Other studies assessed the impact of novelty (Krebs et al., 2017, 2013, 2011), emotion (Lerner et al., 2009; Sterpenich et al., 2006), stress/anger (Gilam et al., 2017; Henckens et al., 2012; van Marle et al., 2010), pain (Brooks et al., 2017; Erpelding et al., 2014; Hubbard et al., 2011; Schulte et al., 2016; Sclocco et al., 2016) and fear/threat (Liddell et al., 2005; Morey et al., 2015; Steuwe et al., 2015, 2014). Studies also investigated the effect of specific interventions on the LC such as vagal nerve stimulation (VNS) (Kraus et al., 2013), light exposure (Vandewalle et al., 2007) and psychotropic medications (Kline et al., 2016; Metzger et al., 2015; Minzenberg et al., 2008). The LC was assessed in healthy participants or in subjects with conditions including nausea (Napadow et al., 2013), cataplexy (Meletti et al., 2015), migraine (Moulton et al., 2014), generalized anxiety disorder (Meeten et al., 2016) and schizophrenia (Anticevic et al., 2014).

A recent review (Sara and Bouret, 2012) proposed that a salient or behavioral significant stimulus (the salient context) activates LC neurons in parallel with autonomic reflex responses, which is in turn modulated by descending inputs from the prefrontal cortex and amygdala (the cognitive context). The relationship between the 'top-down' influence of cortical structures, which plays a role in attentional shifting and behavioral flexibility, and the 'bottom-up' reflexive autonomic response to stimuli is likely to be complex and dynamic. Bearing this in mind, the physiological stimuli and cognitive tasks that generated BOLD activity changes in the LC were divided into two categories to reflect whether the tasks were more likely to demand the recruitment of 'top-down' cognitive processes (for example, if they required attentional set shifting or working memory), or 'bottom-up' mechanisms (i.e. autonomic reflex responses driven by the properties inherent in a stimulus, such as pain). Of the 22 fMRI studies that investigated event-related BOLD activity of the LC, 15 were judged to have used tasks or stimuli that mainly recruited a 'top-down' cognitive process and 13 mainly drove a 'bottom-up' process.

3.3.4 Main findings

The LC was implicated in a wide range of conditions and cognitive functions as described above (see Table 3). The various 'top-down' tasks employed in the BOLD fMRI studies were all judged to involve switching attention in response to stimulus change, consistent with the hypothesized role of the noradrenergic system in shifting between focused and flexible attention (Berridge and Spencer, 2016). All of the 'top-down' tasks increased LC BOLD activity, except one study which reported LC deactivation for such events (Payzan-LeNestour et al., 2013). The LC was also

consistently activated by a range of 'bottom-up' stimuli, all judged to be arousing conditions such as fear/threat, pain, hunger, anger, vagal nerve stimulation, nausea and reward. This is also consistent with the hypothesis that LC neuron firing rates increase during states of high arousal or stress to modulate attention in response to a changing environment (Chandler, 2016; Valentino and Van Bockstaele, 2008). Overall, these findings converge with evidence that the LC is activated by situations that elicit a behavioral orienting response (when ongoing activity is interrupted to face the orienting stimulus (Sara and Bouret, 2012).

There was strong evidence that the LC was functionally connected to the amygdala, as this was reported both in studies where an amygdala or LC seed region was used to investigate whole-brain functional connectivity, and in studies where an amygdala seed region was used to investigate a defined LC region-of-interest (Anticevic et al., 2014; Henckens et al., 2012; Lerner et al., 2009; Meeten et al., 2016; Metzger et al., 2015; van Marle et al., 2010). This is consistent with the known reciprocal connection and interaction between the LC and amygdala for the upregulation of arousal in response to salient or stressful events (Valentino and Van Bockstaele, 2008; Van Bockstaele et al., 1998). Other brain regions functionally connected to the LC included prefrontal cortex (PFC) (Köhler et al., 2016; Minzenberg et al., 2008), hypothalamus (Moulton et al., 2014), cerebellum (Kline et al., 2016; Zhang et al., 2016) hippocampus (Kline et al., 2016; Steuwe et al., 2015), and habenula (Erpelding et al., 2014). Studies have shown that the LC is an important modulator of the PFC, influencing working memory and attention (Berridge and Spencer, 2016; Chandler, 2016). It also provides the sole source

of noradrenaline to the hippocampus (Berridge and Waterhouse, 2003/4), facilitating long-term potentiation and memory encoding (Hu et al., 2007; Klukowski and Harley, 1994).

<<Figure 5a>>

<<Figure 5b>>

As can be seen in Figures 5a and 5b, fMRI studies have reported a range of right and left LC spatial coordinates which contain, but also go substantially beyond, the anatomical boundaries of the LC, as derived from the Keren et al. (2009) coordinates and the known dimensions of the LC based on post-mortem studies (14.5mm in length and 2.5mm in thickness) (Fernandes et al., 2012), shown as solid black points in Figures 5a and 5b. For instance, some of the 95% confidence intervals in the coronal and sagittal planes extend over 10mm, which is several times larger than the anatomical width of the LC. The functional studies that used LC ROI coordinates from Keren et al. (2009) (shown as pink points in Figures 5a and 5b), are more close to the original coordinates compared to studies that did not reference Keren et al. (2009). The upper and lower limits of image acquisition for the Keren et al. (2009) coordinates were the inferior aspect of the red nucleus (MNI z= -18) and the origin of the superior cerebellar peduncle (MNI z= -33), therefore more rostral and caudal sections were not included.

4. Discussion

A variety of structural and functional MRI imaging methods have localized and measured the LC. Here we summarize the key insights from the review, and discuss the degree to which some of the differences in methodological approaches may have limited the sensitivity of the measurement, or the ability to compare/aggregate results across studies. Finally, we conclude with a number of recommendations to optimize the reliability and validity of future LC imaging studies.

4.1 Key insights and methodological issues:

4.1.1 Structural imaging studies

Despite considerable variation in CR among healthy adults, the small number of studies performed in clinical populations (including Parkinson's disease, Alzheimer's disease, MCI, depression and schizophrenia) consistently report a CR reduction in the LC compared to that in healthy controls.

Most studies measured the peak intensity of the LC signal and not an average intensity across the whole volume of the LC. Peak signal intensity was shown to correspond to the position and concentration of LC neurons (Keren et al., 2009) and MRI contrast corresponds to the neuromelanin content of these cells (Keren et al., 2015). Given that cell loss may not affect the whole LC equally and disease-specific patterns of cell loss have been reported (German et al., 1992), it is uncertain whether peak intensity is a reliable estimate for overall LC integrity. Most structural studies prescribed elongated voxels to better capture the known geometry of the LC, hence ensuring minimal partial volume contamination. The largest reported voxel size in LC-optimized MRI studies was

0.5x0.5x3mm^3, which should still provide an adequate resolution to capture neuromelanin content in a structure 2-2.5mm thick and approximately 14.5mm long. One shortcoming of anisotropic voxels is that they may cause strong partial volume effects at the rostral and caudal ends of the LC, as the structure is not perfectly cylindrical and tilted in three dimensions.

Few studies attempted to measure LC volume. Although this could provide an interesting, additional measure of LC integrity that might be useful to study clinical populations where there may be a dissociation between LC volume and signal intensity changes due to accelerated cell death (German et al., 1992), the long-voxel approximation is conceivably less suitable for volume measurements. Partial volume effects could be one reason why the reported volume measurements are almost half the expected value from post-mortem data. The impact of prescribing thinner slices to minimize such errors is yet unclear as all LC-optimized MRI studies that were reviewed reported using slice thickness between 2-3mm.

The differences between the imaging protocols employed may have also led to inconsistencies, but few direct comparisons have been made. Most studies to date used T1-weighted sequences without magnetization preparation, whereas three studies employed inversion recovery based approaches, and the remaining three studies used MT-weighted sequences. It has been suggested that explicit MT preparation might be preferable to enhance neuromelanin content (Chen et al., 2014); it is thought multi-slice RARE sensitivity might only be incidental due to off-resonance MT effects induced by the

23

poor spatial selectivity of refocusing pulses (Nakane et al., 2008). Chen et al. confirmed MT weighting returned greater CNR values in the substantia nigra than T1-TSE scans; however, both acquisitions were found to be on par for LC measurements. It is worth discussing that off-resonance MT pulses and RARE acquisitions result in high specific absorption rates (SAR), often close to the safety limit; this is an important caveat warning most of the *in vivo* prescriptions at 1.5/3T might not be readily available at ultra-high field (i.e. ≥7T).

There is currently an open debate as to whether LC measurements should rely on user intervention or be automated, whether the protocol should include segmentation of the whole structure, or whether intensity values should be extracted from a single voxel to avoid spurious contamination. Chen et al. (2014) argued that automated segmentation methods are less susceptible to error and lead to higher consistency between scans and studies. Chen also argued that use of the single-voxel method, where the voxel with the highest intensity either side of the fourth ventricle is used to localize the LC, is highly susceptible to noise, and suggested that automated segmentation can overcome this problem. In contrast, Keren et al. (2009) argued that assessing single voxels is more reliable than automated or manual segmentation of the LC signal because it is independent of LC boundary definition or signal intensity thresholding, and should reflect the greatest density of LC cells within a section. Keren et al. (2009) explained that the amorphous structure and unclear boundaries of the LC signal, which varied across subjects, would make any segmentation extremely difficult. No study has directly

compared manual and automated methods, and it is not known to what extent multiple, blinded measurements as well as ensuring acceptable levels of inter-rater and intra-rater reliability can compensate for error and inconsistency when using any of these methods.

Normalization of the LC signal intensity to a reference region (most commonly the pontine tegmentum) was not supported by Keren et al. (2009; 2015). This was because the pontine tegmentum showed significant age-related decline in signal, a finding which was also reported in a study of healthy adults (Clewett et al., 2016). Keren et al. (2009) found that older adults were more likely to exhibit a T1 hyperintense signal in the LC in the most caudal sections of the LC (left MNI z= -30, right MNI z=-33), whereas younger adults were more likely to exhibit an LC signal in the most rostral sections (left MNI z= -18, right MNI z= -21). The precise nature of the apparent age-related decline in LC signal intensity has not yet been characterized and the two studies that investigated the effects of ageing provide conflicting results. It has also been suggested that drugs such as nicotine can induce the activation of LC noradrenergic neurons (Tung et al., 1989), and therefore smoking may enhance the signal intensity and should be adjusted for (Sasaki et al., 2008a). However, there are no established methods for doing this and no study published to date has corrected data for age or smoking.

Few studies reported methods to account for the potential effects of subject head motion. The duration of scanning in the majority of structural scans was over 10 minutes and head motion may have reduced image quality, especially in those who may have found it more difficult to lie still in the scanner e.g. patients with PD or AD.

4.1.2 Functional imaging studies

Consistent with animal studies and models of LC function, the LC is activated by a variety of tasks or stimuli that induce stress or involve switching attention in response to stimulus change. Functional connectivity studies showed connectivity to a range of brain regions, with the strongest evidence for the amygdala.

Within functional MRI studies, the distribution of location coordinates is much greater than expected based on the known anatomical shape and location of the LC. Unsurprisingly, variation in LC location coordinates was lowest in studies that used coordinates provided by Keren et al. (2009) to define the LC ROI. However, even among these studies, the reported coordinates involved an area that is larger than the LC based around the Keren et al. (2009) coordinates. Other factors such as poor precision of coregistration, differences in measurement methods, suboptimal resolution, uncorrected physiological noise and LC location variability between individuals could also have contributed to the deviation of reported functional coordinates from the Keren et al. (2009) coordinates. Due to the histological validation on which this study was based and the high voxel resolution involved, it arguably provides a more valid localization method than using previously published functional MRI coordinates. As the upper and lower limits of image acquisition in this study were MNI z= -18 and MNI z= -33 respectively, the validity of reported location coordinates situated more rostrally or caudally to these sections cannot be assessed in the same way. Interestingly, Keren et al. (2009) also showed that with increasing age, peak LC signal intensity shifts from a rostral to a caudal

26

direction, however the relationship between peak LC signal intensity (and greatest concentration of neuromelanin-containing LC neurons) and strength of LC BOLD activity has not been established.

Functional studies acquired imaging data at lower resolutions than structural studies. A larger voxel size (the largest reported was 3.75x3.75x4mm^3) may not accurately reflect the activity of the LC due to a mismatch between the LC size and the size of the voxel. Some functional studies reported resampling the data to achieve a voxel size between 1-2mm^3, but resampling to a smaller voxel size will not improve the acquired resolution.

The small size of the LC poses a challenge to researchers when deciding how to process their imaging data. When used appropriately, the benefits of spatial smoothing include increasing the signal-to-noise ratio and managing the anatomical and functional variation between subjects. However, by allowing adjacent voxels to contribute to the estimated signal, spatial smoothing can also increase the likelihood that the small area of LC BOLD activity is contaminated by noise from surrounding neural tissue. The overall impact of spatial smoothing on study outcomes is uncertain. (Murphy et al., 2014) conducted analyses on both smoothed and unsmoothed data, and showed that although unsmoothed data resulted in more spatially constrained regions of activation, after smoothing the relationship between pupil diameter and LC activity still remained significant.

Most functional studies reported a coregistration method, and a variety of templates and

methods were used. However no study was judged to have adequately assessed the precision of their coregistration. The precision and method of coregistration in fMRI studies is likely to influence the LC location coordinates obtained, as demonstrated in one study (Köhler et al., 2016) which compared using the standard ICBM template with a specialized brainstem and cerebellum template (SUIT). One way of assessing the precision of coregistration between the anatomical and functional LC data, as well as between the LC on the individual scan and the normalized group average, is to compare the 'goodness of fit' between a structural group template and the individual structural images. This manual method allows researchers to check that the group template correctly identifies LC in all subjects, and is an important step to ensure the precise coregistration for small structures such as the LC.

Finally, signals arising from respiratory motion and cardiac pulsatility may attenuate task-related BOLD response in pontine structures and this effect is stronger with increasing field strength. However, only a minority of studies reported correcting imaging data for physiological noise (i.e. cardiac and respiratory signals).

4.2 Adjunctive methods used to measure the LC

Some studies used adjunctive, non-MRI techniques to measure the LC which could potentially add validity to the LC localization process. For example, positron emission tomography (PET) was used to detect the LC by localizing regions containing the norepinephrine transporter (Adhikarla et al., 2016/5). Other PET studies assessed metabolic activity related to wakefulness, which found that LC regional brain glucose

metabolism was higher in the evenings than the morning (Buysse et al., 2004), and that this diurnal increase was smaller in depressed patients (Germain et al., 2007). However, these changes were found in a cluster of midline and brainstem structures and were not specific to the LC.

Pupillometry has been considered to provide a potential indirect measure of human LC activity as this covaried with pupil diameter during performance of an attentional task (Murphy et al., 2014; Sterpenich et al., 2006). Experimental evidence shows increases in pupil diameter are modulated by physiological manipulations that increase the level of arousal, such as noxious stimuli (Chapman et al., 1999; Larson and Talke, 2001; Tassorelli et al., 1995), anxiety (Bakes et al., 1990; Bitsios et al., 2004, 1999), high cognitive load (Steinhauer et al., 2004; Sterpenich et al., 2006) or extreme ambient temperature (Leung et al., 1992). Pharmacological studies show that the LC-directed increase in pupil diameter is likely to be mediated via a contribution from a2-adrenoceptor inhibition on the parasympathetic oculomotor complex (Koss, 1986; Morley et al., 1991; Phillips et al., 2000).

Lower heart rate variability (HRV) was also associated with increased LC activity (Sclocco et al., 2016) and increased LC neuromelanin contrast (Mather et al., 2017). The LC inhibits parasympathetic modulation of the heart (Samuels and Szabadi, 2008a) via the vagus nerve which increases HRV (Laitio T, 2017a, 2017b). Studies have shown that HRV may index the output of an integrated regulatory neural network that responds to threat/stress, which includes the brainstem nuclei, amygdala and prefrontal cortex

(Thayer et al., 2012).

In *ex vivo* studies, histological analysis of brainstem specimens was used to validate the location of the LC (Keren et al., 2009; Sasaki et al., 2006) and to confirm the source of the neuromelanin-signal on MRI (Keren et al., 2015, 2009). Using *ex vivo* data to inform or validate *in vivo* functional neuroimaging studies relies on the assumption that the chemically fixed brain specimens respond in a similar way to living brain tissue under MRI scanning conditions, and that both coregistration procedures have resulted in usable brain templates that are directly comparable.

4.3 Directions for future research:

A number of observations concerning the most valid methods to localize and measure the LC using structural or functioning MRI methods emerge from our review. We have used the available published evidence to highlight where further original research is required (summarized in Table 4).

4.3.1 Structural MRI studies

1) A consistent and valid method to calculate CR should be adopted across structural studies to allow findings to be aggregated and compared. The most commonly adopted CR calculation formula was used to compare findings in this review, thus future studies should ideally report on this metric to enable greater statistical power in meta-analyses.

2) More studies investigating the integrity of the LC in clinical groups are needed,

especially in patients with AD as currently there is only one published structural study that has reported CR data in this group. The CR value has been the most popular outcome measure to reflect LC integrity; fewer studies have reported LC volume, which may also provide a useful measure.

3) Sensitivity and specificity to age-related changes and neurodegenerative conditions could potentially be increased by assessing CR across the rostro-caudal extent of the LC. Rosto-caudal resolution can be improved by using thinner slices than currently used in most studies. Comparisons of LC imaging data to biomarkers (e.g. CSF levels of tau and Aß; molecular imaging) may also provide information on how LC structure is affected in different stages of preclinical AD.

4) Studies should ideally perform a quantitative measure of LC signal intensity (i.e. normalize LC signal intensity to that of a reference region, until a valid non-reference area approach is achieved) to increase the signal to noise ratio. A recent study could show the feasibility of a quantitative imaging approach of the LC, providing a new way to measure the LC without relying on a reference area (Hämmerer et al., 2017, under review). Future studies should also investigate how results can be corrected for participant age and smoking status, and assess the importance of assessor blinding, reference region (pontine) signal intensity variability and partial volume effects.

4.3.2 Functional MRI studies

1) The distribution of location coordinates from functional studies show greater rostral and caudal extension than the coordinates from Keren et al., (2009),

however to our knowledge these locations have not been neuroanatomically validated. Future studies should attempt to shed light on whether this is predominantly due to variation in coregistration methods or differences in LC position across individuals.

2) Due to limitations in the spatial resolution of fMRI, studies should ideally coregister functional images with structural LC templates generated from their sample and report the method and precision of coregistration in detail. Future studies should aim to use the highest possible fMRI resolution and not rely solely on resampling to a higher resolution, which will not improve measurement accuracy. Previously published template maps such as Keren et al., (2009) (available online http://eckertlab.org/LC/) may be useful to assess the accuracy of the LC region-of-interest obtained.

3) Coregistration with specialized templates and spatial smoothing of functional data should be performed with appropriate justification and it is useful to also report outcomes from coregistration with standard templates and unsmoothed data for comparison. Additionally, functional BOLD data should be corrected for physiological noise (cardiac and respiratory signals) as well as head motion to reduce acquisition noise.

4) Future studies should continue to explore task designs and stimuli that may trigger LC activation, and investigate the common cognitive and physiological mechanisms that underlie LC activation. Adjunctive methods such as HRV and pupillometry are promising indirect measures of LC activity and require further study.

4.4 Limitations:

This review focused on studies that used MRI to detect the LC in order to be able to compare scan parameters, preprocessing procedures, as well as resulting signal intensities. We excluded functional studies that did not report location coordinates for the LC, and non-peer reviewed studies including posters and dissertations were also excluded. These excluded studies may have employed other methods or investigated other independent variables that were not reviewed, and inclusion of these results may have altered the results and conclusions of the review. In addition, some studies of LC structure and function may not have reported negative findings which would contribute to publication bias and the potential overestimation in this review of any group differences.

5. Conclusion:

A variety of structural and functional MRI methods have been employed to localize and measure the LC. This methodological variability limits the ability to compare or aggregate results across studies. However, the consistency of findings in certain patient groups using neuromelanin-sensitive MRI is promising; yet demonstrating the overall specificity and sensitivity of this method to age-related changes and neurodegenerative conditions represents a challenge for future studies. The widespread distribution of LC coordinates reported in functional MRI studies suggests that some of the effects might not have been originated in the LC. Only one published study has generated a histologically validated location map of the human LC and future studies that can replicate and extend these results are needed in order to make strong conclusions about the validity of LC

coordinate data from existing and future functional MRI studies.

References

Adhikarla, V., Zeng, F., Votaw, J.R., Goodman, M.M., Nye, J.A., 2016/5. Compartmental modeling of [11C]MENET binding to the norepinephrine transporter in the healthy human brain. Nucl. Med. Biol. 43, 318–323.

Altmann, A., Tian, L., Henderson, V.W., Greicius, M.D., Alzheimer's Disease Neuroimaging Initiative Investigators, 2014. Sex modifies the APOE-related risk of developing Alzheimer disease. Ann. Neurol. 75, 563–573.

Andersen, K., Launer, L.J., Dewey, M.E., Letenneur, L., Ott, A., Copeland, J.R., Dartigues, J.F., Kragh-Sorensen, P., Baldereschi, M., Brayne, C., Lobo, A., Martinez-Lage, J.M., Stijnen, T., Hofman, A., 1999. Gender differences in the incidence of AD and vascular dementia: The EURODEM Studies. EURODEM Incidence Research Group. Neurology 53, 1992–1997.

Anticevic, A., Tang, Y., Cho, Y.T., Repovs, G., Cole, M.W., Savic, A., Wang, F., Krystal, J.H., Xu, K., 2014. Amygdala connectivity differs among chronic, early course, and individuals at risk for developing schizophrenia. Schizophr. Bull. 40, 1105–1116.

Arango, V., Underwood, M.D., Mann, J.J., 1996. Fewer pigmented locus coeruleus neurons in suicide victims: preliminary results. Biol. Psychiatry 39, 112–120.

Bakes, A., Bradshaw, C.M., Szabadi, E., 1990. Attenuation of the pupillary light reflex in anxious patients. Br. J. Clin. Pharmacol. 30, 377–381.

Bär, K.-J., de la Cruz, F., Schumann, A., Koehler, S., Sauer, H., Critchley, H., Wagner, G., 2016. Functional connectivity and network analysis of midbrain and brainstem nuclei. Neuroimage 134, 53–63.

Bernard, R., Kerman, I.A., Thompson, R.C., Jones, E.G., Bunney, W.E., Barchas, J.D., Schatzberg, A.F., Myers, R.M., Akil, H., Watson, S.J., 2011. Altered expression of glutamate signaling, growth factor, and glia genes in the locus coeruleus of patients with major depression. Mol. Psychiatry 16, 634–646.

Berridge, C.W., Spencer, R.C., 2016. Differential cognitive actions of norepinephrine a2 and a1 receptor signaling in the prefrontal cortex. Brain Res. 1641, 189–196.

Berridge, C.W., Waterhouse, B.D., 2003/4. The locus coeruleus–noradrenergic system: modulation of behavioral state and state-dependent cognitive processes. Brain Res. Rev. 42, 33–84.

Bitsios, P., Philpott, A., Langley, R.W., Bradshaw, C.M., Szabadi, E., 1999. Comparison

of the effects of diazepam on the fear-potentiated startle reflex and the fear-inhibited light reflex in man. J. Psychopharmacol. 13, 226–234.

Bitsios, P., Szabadi, E., Bradshaw, C.M., 2004. The fear-inhibited light reflex: importance of the anticipation of an aversive event. Int. J. Psychophysiol. 52, 87–95.

Braak, H., Thal, D.R., Ghebremedhin, E., Del Tredici, K., 2011. Stages of the pathologic process in Alzheimer disease: age categories from 1 to 100 years. J. Neuropathol. Exp. Neurol. 70, 960–969.

Brooks, J.C.W., Davies, W.-E., Pickering, A.E., 2017. Resolving the Brainstem Contributions to Attentional Analgesia. J. Neurosci. 37, 2279–2291.

Buysse, D.J., Nofzinger, E.A., Germain, A., Meltzer, C.C., Wood, A., Ombao, H., Kupfer, D.J., Moore, R.Y., 2004. Regional brain glucose metabolism during morning and evening wakefulness in humans: preliminary findings. Sleep 27, 1245–1254.

Castellanos, G., Fernández-Seara, M.A., Lorenzo-Betancor, O., Ortega-Cubero, S., Puigvert, M., Uranga, J., Vidorreta, M., Irigoyen, J., Lorenzo, E., Muñoz-Barrutia, A., Ortiz-de-Solorzano, C., Pastor, P., Pastor, M.A., 2015. Automated neuromelanin imaging as a diagnostic biomarker for Parkinson's disease. Mov. Disord. 30, 945–952.

Chandler, D.J., 2016. Evidence for a specialized role of the locus coeruleus noradrenergic system in cortical circuitries and behavioral operations. Brain Res. 1641, 197–206.

Chapman, C.R., Oka, S., Bradshaw, D.H., Jacobson, R.C., Donaldson, G.W., 1999. Phasic pupil dilation response to noxious stimulation in normal volunteers: relationship to brain evoked potentials and pain report. Psychophysiology 36, 44–52.

Chen, X., Huddleston, D.E., Langley, J., Ahn, S., Barnum, C.J., Factor, S.A., Levey, A.I., Hu, X., 2014. Simultaneous imaging of locus coeruleus and substantia nigra with a quantitative neuromelanin MRI approach. Magn. Reson. Imaging 32, 1301–1306.

Clewett, D.V., Lee, T.-H., Greening, S., Ponzio, A., Margalit, E., Mather, M., 2016. Neuromelanin marks the spot: identifying a locus coeruleus biomarker of cognitive reserve in healthy aging. Neurobiol. Aging 37, 117–126.

Costafreda, S.G., Fu, C.H.Y., Lee, L., Everitt, B., Brammer, M.J., David, A.S., 2006. A systematic review and quantitative appraisal of fMRI studies of verbal fluency: role of the left inferior frontal gyrus. Hum. Brain Mapp. 27, 799–810.

D. M. A. Mann P. O. Yates, 1974. Lipoprotein Pigments—Their Relationship to Ageing in the Human Nervous System<subtitle>II. The Melanin Content of Pigmented Nerve Cells</subtitle>. Brain. doi:10.1093/brain/97.3.489

Ehrminger, M., Latimier, A., Pyatigorskaya, N., Garcia-Lorenzo, D., Leu-Semenescu, S., Vidailhet, M., Lehericy, S., Arnulf, I., 2016. The coeruleus/subcoeruleus complex in idiopathic rapid eye movement sleep behaviour disorder. Brain 139, 1180–1188.

Enochs, W.S., Petherick, P., Bogdanova, A., Mohr, U., Weissleder, R., 1997. Paramagnetic metal scavenging by melanin: MR imaging. Radiology 204, 417–423.

Erpelding, N., Sava, S., Simons, L.E., Lebel, A., Serrano, P., Becerra, L., Borsook, D., 2014. Habenula functional resting-state connectivity in pediatric CRPS. J. Neurophysiol. 111, 239–247.

Fernandes, P., Regala, J., Correia, F., Gonçalves-Ferreira, A.J., 2012. The human locus coeruleus 3-D stereotactic anatomy. Surg. Radiol. Anat. 34, 879–885.

García-Lorenzo, D., Longo-Dos Santos, C., Ewenczyk, C., Leu-Semenescu, S., Gallea, C., Quattrocchi, G., Pita Lobo, P., Poupon, C., Benali, H., Arnulf, I., Vidailhet, M., Lehericy, S., 2013. The coeruleus/subcoeruleus complex in rapid eye movement sleep behaviour disorders in Parkinson's disease. Brain 136, 2120–2129.

Germain, A., Nofzinger, E.A., Meltzer, C.C., Wood, A., Kupfer, D.J., Moore, R.Y., Buysse, D.J., 2007. Diurnal variation in regional brain glucose metabolism in depression. Biol. Psychiatry 62, 438–445.

German, D.C., Manaye, K.F., White, C.L., 3rd, Woodward, D.J., McIntire, D.D., Smith, W.K., Kalaria, R.N., Mann, D.M., 1992. Disease-specific patterns of locus coeruleus cell loss. Ann. Neurol. 32, 667–676.

Gilam, G., Lin, T., Fruchter, E., Hendler, T., 2017. Neural indicators of interpersonal anger as cause and consequence of combat training stress symptoms. Psychol. Med. 1–12.

Grudzien, A., Shaw, P., Weintraub, S., Bigio, E., Mash, D.C., Mesulam, M.M., 2007. Locus coeruleus neurofibrillary degeneration in aging, mild cognitive impairment and early Alzheimer's disease. Neurobiol. Aging 28, 327–335.
Hämmerer, D., Callaghan, MF., Cardenas-Blanco, A., Kosciessa, J.,Weiskopf, N, Dolan, RJ., Düzel, E., 2017. Quantitative multi-parameter mapping of locus coeruleus and substantia nigra integrity in ageing. *Under review.*

Henckens, M.J.A.G., van Wingen, G.A., Joëls, M., Fernández, G., 2012. Corticosteroid induced decoupling of the amygdala in men. Cereb. Cortex 22, 2336–2345.

Hubbard, C.S., Labus, J.S., Bueller, J., Stains, J., Suyenobu, B., Dukes, G.E., Kelleher, D.L., Tillisch, K., Naliboff, B.D., Mayer, E.A., 2011. Corticotropin-releasing factor receptor 1 antagonist alters regional activation and effective connectivity in an emotional-arousal circuit during expectation of abdominal pain. J. Neurosci. 31, 12491–12500.

Hu, H., Real, E., Takamiya, K., Kang, M.-G., Ledoux, J., Huganir, R.L., Malinow, R., 2007. Emotion enhances learning via norepinephrine regulation of AMPA-receptor trafficking. Cell 131, 160–173.

Isaias, I.U., Trujillo, P., Summers, P., Marotta, G., Mainardi, L., Pezzoli, G., Zecca, L., Costa, A., 2016. Neuromelanin Imaging and Dopaminergic Loss in Parkinson's Disease. Front. Aging Neurosci. 8, 196.

Kahnt, T., Tobler, P.N., 2013. Salience signals in the right temporoparietal junction facilitate value-based decisions. J. Neurosci. 33, 863–869.

Keren, N.I., Lozar, C.T., Harris, K.C., Morgan, P.S., Eckert, M.A., 2009. In vivo mapping of the human locus coeruleus. Neuroimage 47, 1261–1267.

Keren, N.I., Taheri, S., Vazey, E.M., Morgan, P.S., Granholm, A.-C.E., Aston-Jones, G.S., Eckert, M.A., 2015. Histologic validation of locus coeruleus MRI contrast in post-mortem tissue. Neuroimage 113, 235–245.

Kline, R.L., Zhang, S., Farr, O.M., Hu, S., Zaborszky, L., Samanez-Larkin, G.R., Li, C.-S.R., 2016. The Effects of Methylphenidate on Resting-State Functional Connectivity of the Basal Nucleus of Meynert, Locus Coeruleus, and Ventral Tegmental Area in Healthy Adults. Front. Hum. Neurosci. 10, 149.

Klukowski, G., Harley, C.W., 1994. Locus coeruleus activation induces perforant path-evoked population spike potentiation in the dentate gyrus of awake rat. Exp. Brain

Res. 102, 165–170.

Köhler, S., Bär, K.-J., Wagner, G., 2016. Differential involvement of brainstem noradrenergic and midbrain dopaminergic nuclei in cognitive control. Hum. Brain Mapp. 37, 2305–2318.

Koss, M.C., 1986. Pupillary dilation as an index of central nervous system alpha 2-adrenoceptor activation. J. Pharmacol. Methods 15, 1–19.

Kraus, T., Kiess, O., Hösl, K., Terekhin, P., Kornhuber, J., Forster, C., 2013. CNS BOLD fMRI Effects of Sham-Controlled Transcutaneous Electrical Nerve Stimulation in the Left Outer Auditory Canal – A Pilot Study. Brain Stimulation: Basic, Translational, and Clinical Research in Neuromodulation 6, 798–804.

Krebs, R.M., Fias, W., Achten, E., Boehler, C.N., 2013. Picture novelty attenuates semantic interference and modulates concomitant neural activity in the anterior cingulate cortex and the locus coeruleus. Neuroimage 74, 179–187.

Krebs, R.M., Heipertz, D., Schuetze, H., Duzel, E., 2011. Novelty increases the mesolimbic functional connectivity of the substantia nigra/ventral tegmental area (SN/VTA) during reward anticipation: Evidence from high-resolution fMRI. Neuroimage 58, 647–655.

Krebs, R.M., Park, H.R.P., Bombeke, K., Boehler, C.N., 2017. Modulation of locus coeruleus activity by novel oddball stimuli. Brain Imaging Behav. doi:10.1007/s11682-017-9700-4

Lacadie, C.M., Fulbright, R.K., Rajeevan, N., Constable, R.T., Papademetris, X., 2008. More accurate Talairach coordinates for neuroimaging using non-linear registration. Neuroimage 42, 717–725.

Laitio T, J.J., 2017a. The Role of Heart Rate Variability in Risk Stratification for Adverse Postoperative Cardiac Events.

Laitio T, J.J., 2017b. The Role of Heart Rate Variability in Risk Stratification for Adverse Postoperative Cardiac Events.

Langley, J., Huddleston, D.E., Liu, C.J., Hu, X., 2016. Reproducibility of locus coeruleus and substantia nigra imaging with neuromelanin sensitive MRI. MAGMA. doi:10.1007/s10334-016-0590-z

Larson, M.D., Talke, P.O., 2001. Effect of dexmedetomidine, an alpha2-adrenoceptor agonist, on human pupillary reflexes during general anaesthesia. Br. J. Clin. Pharmacol. 51, 27–33.

Laureiro-Martínez, D., Brusoni, S., Canessa, N., Zollo, M., 2015. Understanding the exploration–exploitation dilemma: An fMRI study of attention control and decision-making performance. Strat. Mgmt. J. 36, 319–338.

Lerner, Y., Papo, D., Zhdanov, A., Belozersky, L., Hendler, T., 2009. Eyes wide shut: amygdala mediates eyes-closed effect on emotional experience with music. PLoS One 4, e6230.

Leung, N.K., Bradshaw, C.M., Szabadi, E., 1992. Effect of high ambient temperature on the kinetics of the pupillary light reflex in healthy volunteers. Br. J. Clin. Pharmacol. 33, 458–460.

Liddell, B.J., Brown, K.J., Kemp, A.H., Barton, M.J., Das, P., Peduto, A., Gordon, E., Williams, L.M., 2005. A direct brainstem-amygdala-cortical "alarm" system for subliminal signals of fear. Neuroimage 24, 235–243.

Lohr, J.B., Jeste, D.V., 1988. Locus ceruleus morphometry in aging and schizophrenia. Acta Psychiatr. Scand. 77, 689–697.

Manaye, K.F., McIntire, D.D., Mann, D.M., German, D.C., 1995. Locus coeruleus cell loss in the aging human brain: a non-random process. J. Comp. Neurol. 358, 79–87.

Mann, D.A., 1983. The locus coeruleus and its possible role in aging and degenerative disease of the human central nervous system.

Mather, M., Harley, C.W., 2016. The Locus Coeruleus: Essential for Maintaining Cognitive Function and the Aging Brain. Trends Cogn. Sci. 20, 214–226.

Mather, M., Joo Yoo, H., Clewett, D.V., Lee, T.-H., Greening, S.G., Ponzio, A., Min, J., Thayer, J.F., 2017. Higher locus coeruleus MRI contrast is associated with lower parasympathetic influence over heart rate variability. Neuroimage 150, 329–335.

Matsuura, K., Maeda, M., Yata, K., Ichiba, Y., Yamaguchi, T., Kanamaru, K., Tomimoto, H., 2013. Neuromelanin magnetic resonance imaging in Parkinson's disease and multiple system atrophy. Eur. Neurol. 70, 70–77.

Meeten, F., Davey, G.C.L., Makovac, E., Watson, D.R., Garfinkel, S.N., Critchley, H.D., Ottaviani, C., 2016. Goal Directed Worry Rules Are Associated with Distinct Patterns of Amygdala Functional Connectivity and Vagal Modulation during Perseverative Cognition. Front. Hum. Neurosci. 10, 553.

Mehler, M.F., Purpura, D.P., 2009. Autism, fever, epigenetics and the locus coeruleus. Brain Res. Rev. 59, 388–392.

Meletti, S., Vaudano, A.E., Pizza, F., Ruggieri, A., Vandi, S., Teggi, A., Franceschini, C., Benuzzi, F., Nichelli, P.F., Plazzi, G., 2015. The Brain Correlates of Laugh and Cataplexy in Childhood Narcolepsy. J. Neurosci. 35, 11583–11594.

Metzger, C.D., Wiegers, M., Walter, M., Abler, B., Graf, H., 2015. Local and Global Resting State Activity in the Noradrenergic and Dopaminergic Pathway Modulated by Reboxetine and Amisulpride in Healthy Subjects. Int. J. Neuropsychopharmacol. 19. doi:10.1093/ijnp/pyv080

Minzenberg, M.J., Watrous, A.J., Yoon, J.H., Ursu, S., Carter, C.S., 2008. Modafinil shifts human locus coeruleus to low-tonic, high-phasic activity during functional MRI. Science 322, 1700–1702.

Miyoshi, F., Ogawa, T., Kitao, S.-I., Kitayama, M., Shinohara, Y., Takasugi, M., Fujii, S., Kaminou, T., 2013. Evaluation of Parkinson disease and Alzheimer disease with the use of neuromelanin MR imaging and (123)I-metaiodobenzylguanidine scintigraphy. AJNR Am. J. Neuroradiol. 34, 2113–2118.

Mohanty, A., Gitelman, D.R., Small, D.M., Mesulam, M.M., 2008. The spatial attention network interacts with limbic and monoaminergic systems to modulate motivation-induced attention shifts. Cereb. Cortex 18, 2604–2613.

Morey, R.A., Dunsmoor, J.E., Haswell, C.C., Brown, V.M., Vora, A., Weiner, J., Stjepanovic, D., Wagner, H.R., 3rd, VA Mid-Atlantic MIRECC Workgroup, LaBar, K.S., 2015. Fear learning circuitry is biased toward generalization of fear associations in posttraumatic stress disorder. Transl. Psychiatry 5, e700.

Morley, M.J., Bradshaw, C.M., Szabadi, E., 1991. Effects of clonidine and yohimbine on the pupillary light reflex and carbachol-evoked sweating in healthy volunteers. Br. J. Clin. Pharmacol. 31, 99–101.

Moulton, E.A., Becerra, L., Johnson, A., Burstein, R., Borsook, D., 2014. Altered

Hypothalamic Functional Connectivity with Autonomic Circuits and the Locus Coeruleus in Migraine. PLoS One 9, e95508.

Mukai, M., Sugaya, K., Yabe, I., Goto, Y.-I., Yokochi, F., Miyamoto, K., Cai, H., Sasaki, H., Matsubara, S., 2013. Neuromelanin MRI in a family with mitochondrial parkinsonism harboring a Y955C mutation in POLG1. Parkinsonism Relat. Disord. 19, 821–824.

Murphy, P.R., O'Connell, R.G., O'Sullivan, M., Robertson, I.H., Balsters, J.H., 2014. Pupil diameter covaries with BOLD activity in human locus coeruleus. Hum. Brain Mapp. 35, 4140–4154.

Nakane, T., Nihashi, T., Kawai, H., Naganawa, S., 2008. Visualization of neuromelanin in the Substantia nigra and locus ceruleus at 1.5T using a 3D-gradient echo sequence with magnetization transfer contrast. Magn. Reson. Med. Sci. 7, 205–210.

Napadow, V., Sheehan, J.D., Kim, J., Lacount, L.T., Park, K., Kaptchuk, T.J., Rosen, B.R., Kuo, B., 2013. The brain circuitry underlying the temporal evolution of nausea in humans. Cereb. Cortex 23, 806–813.

Neufang, S., Geiger, M.J., Homola, G.A., Mahr, M., Akhrif, A., Nowak, J., Reif, A., Romanos, M., Deckert, J., Solymosi, L., Domschke, K., 2015. Modulation of prefrontal functioning in attention systems by NPSR1 gene variation. Neuroimage 114, 199–206.

Ohtsuka, C., Sasaki, M., Konno, K., Kato, K., Takahashi, J., Yamashita, F., Terayama, Y., 2014. Differentiation of early-stage parkinsonisms using neuromelanin-sensitive magnetic resonance imaging. Parkinsonism Relat. Disord. 20, 755–760.

Ohtsuka, C., Sasaki, M., Konno, K., Koide, M., Kato, K., Takahashi, J., Takahashi, S., Kudo, K., Yamashita, F., Terayama, Y., 2013. Changes in substantia nigra and locus coeruleus in patients with early-stage Parkinson's disease using neuromelanin-sensitive MR imaging. Neurosci. Lett. 541, 93–98.

Payzan-LeNestour, E., Dunne, S., Bossaerts, P., O'Doherty, J.P., 2013. The Neural Representation of Unexpected Uncertainty during Value-Based Decision Making. Neuron 79, 191–201.

Phillips, M.A., Szabadi, E., Bradshaw, C.M., 2000. Comparison of the effects of clonidine and yohimbine on pupillary diameter at different illumination levels. Br. J. Clin. Pharmacol. 50, 65–68.

Raizada, R.D.S., Poldrack, R.A., 2007. Challenge-driven attention: interacting frontal and brainstem systems. Front. Hum. Neurosci. 1, 3.

Ressler, K.J., Nemeroff, C.B., 1999. Role of norepinephrine in the pathophysiology and treatment of mood disorders. Biol. Psychiatry 46, 1219–1233.

Samuels, E.R., Szabadi, E., 2008a. Functional neuroanatomy of the noradrenergic locus coeruleus: its roles in the regulation of arousal and autonomic function part I: principles of functional organisation. Curr. Neuropharmacol. 6, 235–253.

Samuels, E.R., Szabadi, E., 2008b. Functional neuroanatomy of the noradrenergic locus coeruleus: its roles in the regulation of arousal and autonomic function part II: physiological and pharmacological manipulations and pathological alterations of locus coeruleus activity in humans. Curr. Neuropharmacol. 6, 254–285.

Sara, S.J., 2009. The locus coeruleus and noradrenergic modulation of cognition. Nat. Rev. Neurosci. 10, 211–223.

Sara, S.J., Bouret, S., 2012. Orienting and reorienting: the locus coeruleus mediates cognition through arousal. Neuron 76, 130–141.

Sasaki, M., Shibata, E., Kudo, K., Tohyama, K., 2008a. Neuromelanin-Sensitive MRI. Clin. Neuroradiol. 18, 147–153.

Sasaki, M., Shibata, E., Ohtsuka, K., Endoh, J., Kudo, K., Narumi, S., Sakai, A., 2010. Visual discrimination among patients with depression and schizophrenia and healthy individuals using semiquantitative color-coded fast spin-echo T1-weighted magnetic resonance imaging. Neuroradiology 52, 83–89.

Sasaki, M., Shibata, E., Tohyama, K., Kudo, K., Endoh, J., Otsuka, K., Sakai, A., 2008b. Monoamine neurons in the human brain stem: anatomy, magnetic resonance imaging findings, and clinical implications. Neuroreport 19, 1649–1654.

Sasaki, M., Shibata, E., Tohyama, K., Takahashi, J., Otsuka, K., Tsuchiya, K., Takahashi, S., Ehara, S., Terayama, Y., Sakai, A., 2006. Neuromelanin magnetic resonance imaging of locus ceruleus and substantia nigra in Parkinson's disease. Neuroreport 17, 1215–1218.

Schilbach, L., Eickhoff, S.B., Cieslik, E., Shah, N.J., Fink, G.R., Vogeley, K., 2011. Eyes on me: an fMRI study of the effects of social gaze on action control. Soc. Cogn. Affect. Neurosci. 6, 393–403.

Schulte, L.H., Sprenger, C., May, A., 2016. Physiological brainstem mechanisms of trigeminal nociception: An fMRI study at 3T. Neuroimage 124, 518–525.

Schwarz, 2012. T1-Weighted MRI shows stage-dependent substantia nigra signal loss in Parkinson's disease. Mov. Disord. 27, 335–335.

Schwarz, S.T., Xing, Y., Tomar, P., Bajaj, N., Auer, D.P., 2016. In Vivo Assessment of Brainstem Depigmentation in Parkinson Disease: Potential as a Severity Marker for Multicenter Studies. Radiology 160662.

Sclocco, R., Beissner, F., Desbordes, G., Polimeni, J.R., Wald, L.L., Kettner, N.W., Kim, J., Garcia, R.G., Renvall, V., Bianchi, A.M., Cerutti, S., Napadow, V., Barbieri, R., 2016. Neuroimaging brainstem circuitry supporting cardiovagal response to pain: a combined heart rate variability/ultrahigh-field (7 T) functional magnetic resonance imaging study. Philos. Trans. A Math. Phys. Eng. Sci. 374. doi:10.1098/rsta.2015.0189

Shibata, E., Sasaki, M., Tohyama, K., Kanbara, Y., Otsuka, K., Ehara, S., Sakai, A., 2006. Age-related changes in locus ceruleus on neuromelanin magnetic resonance imaging at 3 Tesla. Magn. Reson. Med. Sci. 5, 197–200.

Shibata, E., Sasaki, M., Tohyama, K., Otsuka, K., Endoh, J., Terayama, Y., Sakai, A., 2008. Use of Neuromelanin-Sensitive MRI to Distinguish Schizophrenic and Depressive Patients and Healthy Individuals Based on Signal Alterations in the Substantia Nigra and Locus Ceruleus. Biol. Psychiatry 64, 401–406.

Shibata, E., Sasaki, M., Tohyama, K., Otsuka, K., Sakai, A., 2007. Reduced signal of locus ceruleus in depression in quantitative neuromelanin magnetic resonance imaging. Neuroreport 18, 415–418.

Steinhauer, S.R., Siegle, G.J., Condray, R., Pless, M., 2004. Sympathetic and parasympathetic innervation of pupillary dilation during sustained processing. Int. J. Psychophysiol. 52, 77–86.

Sterpenich, V., D'Argembeau, A., Desseilles, M., Balteau, E., Albouy, G., Vandewalle,

G., Degueldre, C., Luxen, A., Collette, F., Maquet, P., 2006. The locus ceruleus is involved in the successful retrieval of emotional memories in humans. J. Neurosci. 26, 7416–7423.

Steuwe, C., Daniels, J.K., Frewen, P.A., Densmore, M., Pannasch, S., Beblo, T., Reiss, J., Lanius, R.A., 2014. Effect of direct eye contact in PTSD related to interpersonal trauma: an fMRI study of activation of an innate alarm system. Soc. Cogn. Affect. Neurosci. 9, 88–97.

Steuwe, C., Daniels, J.K., Frewen, P.A., Densmore, M., Theberge, J., Lanius, R.A., 2015. Effect of direct eye contact in women with PTSD related to interpersonal trauma: Psychophysiological interaction analysis of connectivity of an innate alarm system. Psychiatry Res. 232, 162–167.

Takahashi, J., Shibata, T., Sasaki, M., Kudo, M., Yanezawa, H., Obara, S., Kudo, K., Ito, K., Yamashita, F., Terayama, Y., 2015. Detection of changes in the locus coeruleus in patients with mild cognitive impairment and Alzheimer's disease: high-resolution fast spin-echo T1-weighted imaging. Geriatr. Gerontol. Int. 15, 334–340.

Tassorelli, C., Micieli, G., Osipova, V., Rossi, F., Nappi, G., 1995. Pupillary and cardiovascular responses to the cold-pressor test. J. Auton. Nerv. Syst. 55, 45–49.

Thayer, J.F., Ahs, F., Fredrikson, M., Sollers, J.J., 3rd, Wager, T.D., 2012. A meta-analysis of heart rate variability and neuroimaging studies: implications for heart rate variability as a marker of stress and health. Neurosci. Biobehav. Rev. 36, 747–756.

Theofilas, P., Ehrenberg, A.J., Dunlop, S., Di Lorenzo Alho, A.T., Nguy, A., Leite, R.E.P., Rodriguez, R.D., Mejia, M.B., Suemoto, C.K., Ferretti-Rebustini, R.E.D.L., Polichiso, L., Nascimento, C.F., Seeley, W.W., Nitrini, R., Pasqualucci, C.A., Jacob Filho, W., Rueb, U., Neuhaus, J., Heinsen, H., Grinberg, L.T., 2016. Locus coeruleus volume and cell population changes during Alzheimer's disease progression: A stereological study in human postmortem brains with potential implication for early-stage biomarker discovery. Alzheimers. Dement. doi:10.1016/j.jalz.2016.06.2362

Trujillo, P., Summers, P.E., Ferrari, E., Zucca, F.A., Sturini, M., Mainardi, L.T., Cerutti, S., Smith, A.K., Smith, S.A., Zecca, L., Costa, A., 2016. Contrast mechanisms associated with neuromelanin-MRI. Magn. Reson. Med. doi:10.1002/mrm.26584

Tung, C.S., Ugedo, L., Grenhoff, J., Engberg, G., Svensson, T.H., 1989. Peripheral induction of burst firing in locus coeruleus neurons by nicotine mediated via excitatory amino acids. Synapse 4, 313–318.

Valentino, R.J., Van Bockstaele, E., 2008. Convergent regulation of locus coeruleus activity as an adaptive response to stress. Eur. J. Pharmacol. 583, 194–203.

Van Bockstaele, E.J., Colago, E.E., Valentino, R.J., 1998. Amygdaloid corticotropin-releasing factor targets locus coeruleus dendrites: substrate for the co-ordination of emotional and cognitive limbs of the stress response. J. Neuroendocrinol. 10, 743–757.

Vandewalle, G., Schmidt, C., Albouy, G., Sterpenich, V., Darsaud, A., Rauchs, G., Berken, P.-Y., Balteau, E., Degueldre, C., Luxen, A., Maquet, P., Dijk, D.-J., 2007. Brain responses to violet, blue, and green monochromatic light exposures in humans: prominent role of blue light and the brainstem. PLoS One 2, e1247.

van Marle, H.J.F., Hermans, E.J., Qin, S., Fernández, G., 2010. Enhanced resting-state connectivity of amygdala in the immediate aftermath of acute psychological stress.

Neuroimage 53, 348–354.

von der Gablentz, J., Tempelmann, C., Münte, T.F., Heldmann, M., 2015. Performance monitoring and behavioral adaptation during task switching: an fMRI study. Neuroscience 285, 227–235.

Watanabe, Y., Tanaka, H., Tsukabe, A., Kunitomi, Y., Nishizawa, M., Hashimoto, R., Yamamori, H., Fujimoto, M., Fukunaga, M., Tomiyama, N., 2014. Neuromelanin magnetic resonance imaging reveals increased dopaminergic neuron activity in the substantia nigra of patients with schizophrenia. PLoS One 9, e104619.

Xuan, B., Mackie, M.-A., Spagna, A., Wu, T., Tian, Y., Hof, P.R., Fan, J., 2016. The activation of interactive attentional networks. Neuroimage 129, 308–319.

Yamamoto, K., Hornykiewicz, O., 2004. Proposal for a noradrenaline hypothesis of schizophrenia. Prog. Neuropsychopharmacol. Biol. Psychiatry 28, 913–922.

Zarow, C., Lyness, S.A., Mortimer, J.A., Chui, H.C., 2003. Neuronal loss is greater in the locus coeruleus than nucleus basalis and substantia nigra in Alzheimer and Parkinson diseases. Arch. Neurol. 60, 337–341.

Zhang, S., Hu, S., Chao, H.H., Li, C.-S.R., 2016. Resting-State Functional Connectivity of the Locus Coeruleus in Humans: In Comparison with the Ventral Tegmental Area/Substantia Nigra Pars Compacta and the Effects of Age. Cereb. Cortex 26, 3413–3427.

<u>Figure captions:</u>

Figure 1. Reconstruction of a human pair of locus coeruleus, shown in the coronal plane. Reprinted with permission from 'The human locus coeruleus 3-D stereotactic anatomy' by P. Fernandez et al., 2012, Surg Radiol Anat 34:879-885. © Springer-Verlag 2012.

Figure 2. Visualization of human LC as a hyperintense signal in the rostral brainstem using T1-weighted MRI optimized to enhance neuromelanin content, seen in axial (B) and coronal (C) planes acquired as shown in (A). Reprinted with permission from Hämmerer et al., 2017 (under review).

Figure 3: PRISMA flow diagram

Figure 4: Mean and median CR values reported by structural MRI studies for each participant group. The weighted mean (middle horizontal line) and 95% confidence intervals (top and bottom horizontal lines) are shown. No weighted mean or confidence interval was constructed for the AD group as only one CR study could be included. Blue points represent median CR and red points represent mean CR. HC=healthy controls, MD=major depression, SZ=schizophrenia, PD=Parkinson disease, AD=Alzheimer's disease, MCI=Mild Cognitive Impairment.

Figure 5a: Peak activations (MNI x,y,z) reported by functional MRI studies for the right LC
Figure 5b: Peak activations (MNI x,y,z) reported by functional MRI studies for the left LC
Figures 5a and 5b show the distribution of the peak activations and hence LC location (MNI coordinates) reported in the fMRI studies, plotted on the coronal, sagittal and transverse planes for the right and left LC respectively. The size of the points are weighted according to sample size. The solid black points represent the ex-vivo location coordinates of the LC obtained using histological specimens to validate the neuromelanin signal (Keren et al., 2009) and the pink points represent the functional MRI studies that reported using Keren et al., (2009) to obtain the LC ROI. The weighted means (middle vertical lines) and bootstrap 95% confidence intervals (left and right vertical lines) are shown for the four bins divided along the range of reported z-coordinates, in the coronal and sagittal planes. Each bin contains 9-10 studies (right side) or 8 studies (left side).

Table 1. LC studies that used structural MRI

Study	Study design	Independent variable	Population sampled	Age range (mean) in yrs	N (%F)	MRI magnet strength	Coregistration method	Identification of LC (manual segmentation unless stated otherwise)	Adjunctive non-MRI methods	Main LC findings and outcome measures (SI, CR, coordinates) $CR_{LC}=(SI_{LC}-SI_{ref})/SI_{ref}$ was used unless stated otherwise
Neuromelanin-optimized T1-weighted MRI										
Astafiev 2010	Cross-sectional	-	HA	-(-)	10 (-)	3T	Individual images were registered to a brainstem atlas template and a group average neuromelanin image was computed.	On axial images, the LC appeared as an area of high signal intensity in the upper pontine teg-mentum immediately anterolateral to the floor of the fourth ventricle	N	MNI location coordinates obtained from area of LC signal intensity. Variability was greatest along the dorsocaudal axis. L =(-3.2, -38.2, -24.8) R= (5.4, -37.9,-24.7)
Castellanos 2015	Case-control	MCI/Dementia (PD)	PD, HC	47-75 (63)	73 (40)	3T	NM-sensitive images were coregistered to the T1 anatomical images, which in turn were coregistered to SPM T1 canonical template. Each atlas image was registered to the target NM-image independently using Elastix.	Fully automated segmentation using reference atlas of 14 manually segmented NM images by an experienced physician.	N	Reduced LC volume in PD vs HC. Median LC volume (mm3): HC=15.2, PD subtypes=8.2-11.9
Chen 2014	Cross-sectional	-	HA	20-50 (-)	6 (50)	3T	For each subject, imaging data analysed using AFNI. All images from the multiple measurements were registered to the first one then averaged.	1) The apex of the 4th ventricle was identified 2)Target ROIs for both the left and right LCs were defined based on the landmarks from a previous histological study (German 1992): two circular ROIs with radius of 3 mm, centered 3 mm left/right and 2 mm posterior to the apex of the 4th ventricle 3)Voxels within the target ROIs whose intensity is equal to	N	For the LC, there was no significant difference in estimations of mean CNR and volume among the GRE-MTC-300, GRE-MTC-300-PKC and RARE sequence. Only graphical data presented. Mean CNR(L+R) appears to range between 6-8.7. Mean volume (L+R) appears to range between 1.8-

								or higher than mean (SI)+4×SD(SI) were considered to be part of the LC.		8.8mm^3 $$CNR = (SI_{LC}-SI_{ref})/SD_{ref}$$
Clewett 2016	Cross-sectional	Age	HA	18-75 (42)	56 (41)	3T	None reported.	Peak NM signal at the corner of 4th ventricle in one slice (ROI size 3x3voxels). Mean SI from R+L ROIs averaged.	N	Higher CNR in older vs younger adults, and in men vs women. CNR positively associated with cognitive reserve score. Mean CNR: Older adults=0.18, younger adults=0.15 $CNR=(SI_{LC}-SI_{PT})/SI_{PT}$
Ehrminger 2016	Case-control	Sleep disorder (RBD)	RBD, HC	- (67)	42 (26)	3T	Identical to Garcia-Lorenzo (2013). ICBM region was resampled onto T1-weighted NM images with rigid and non-linear transformations	ICBM template to define LC, SI calculated from brightest 10 connected voxels	N	Reduced SI in RBD vs HC. Mean (median) SI of LC (R+L): RBD=122.2 (122.4) HC=128.2 (128.1), SI of reference region=100. *[For comparison, mean CR(%): RBD=22.2, HC=28.2]*
Garcia-Lorenzo (I) 2013	Case-control	MCI/Dementia and sleep disorder(PD +/- RBD)	PD (+/- RBD), HC	-(60)	55 (40)	3T	Each NM-sensitive image was registered to the 3D T1-weighted anatomical images	Average intensity of brightest 10 connected voxels in a 700m3 box region defined on ICBM template	Y [e]	Reduced SI in PD with RBD vs PD without RBD and HC. Only graphical data presented. Median SI appears to be approx HC=1.25, PD+RBD = 1.22, PD-RBD=1.27 Reference regions for all subjects were normalized to make SI comparable.
Isaias 2016	Case-control	MCI/Dementia (PD)	PD, HC *pd=46-77*	46-77 (-)	36 (33)	3T	None reported.	Highest intensity voxel adjacent to 4th ventricle. For 3 consecutive slices, SI[LC]= SI of this voxel and its 4 abutting voxels in the image plane.	Y [d]	Reduced CNR in PD vs HC. Mean CNR: PD=3.5(L) 3.9(R), HC=4.9(L) 5.1(R) $CNR=(SI_{LC}-SI_{PT})/SD_{PT}$
Keren 2009	Cross-sectional	-	HA	19-79 (49)	44 (36)	3T	A brainstem template was created by normalizing each cropped brainstem image using SPM5, normalized images were	Peak NM signals on each brainstem axial slice aggregated to create probability map of LC location	Y [c]	Ex vivo, validation of NM-MRI as a technique to measure LC neurones, created an in vivo anatomical map of LC.

							averaged and then normalized into MNI space.			Variance of LC peak signal increases in lower sections. Mean LC spatial location for each section: L (-2.5, -36.3, -18), (-3.1, -36.7, -21), (-3.7, -37.0, -24), (-4.7, -37.3, -27), (-5.5, -37.8, -30), (-6.9, -38.6, -33). R (4.1, -36.2, -18), (4.6, -36.6, -21), (5.2, -36.9, -24), (5.8, -37.2, -27), (6.4, -37.7, -30), 7.6, -37.5, -33).
Keren 2015	Cross-sectional	-	AD, LBD	62-91 (76)	7 (57)	7T	Histologic images were coregistered to the MRI images.	High NM signal at the corner of 4th ventricle (manual)	Y [c]	NM-MRI contrast corresponds to NM in LC neurones. Ex vivo, no numerical data reported
Langley 2016	Cross-sectional	-	HA	-(28)	11 (9)	3T	For each subject, images from 7 GRE measurements were registered to the first image using linear transformation using FSL FLIRT tool and averaged. Volumes were transformed into MNI space: brain extracted T1 weighted images were aligned with MNI brain extracted image using affine transformation.Nonlinear transformation from individual to common space. Individual LC mask transformed to T1 weighted images and common space for each subject.	LC volumes were delineated using a semi-automated thresholding method based on previous anatomical landmarks (Chen 2014). Thresholds were calculated using the mean (μREF), and standard deviation (σREF), of a reference region placed in the cerebral peduncle. Voxels with SI>μREF+4σREF were considered to be LC.	N	High reproducibility of MT contrast and LC volume using this method. Only graphical data presented. Volumes appear to range between approx 10-30mm^3 . MT contrast (%) appears to range between 18-26. MT contrast=(SI$_{voxel}$-SI$_{ref}$)/SI$_{ref}$
Mather 2017	Cross-sectional	Age, HRV	HA	18-75 (HYA 24, HOA 68)	45 (40)	3T	None reported.	Centre of cross (1.3mm or 3 voxels wide) manually placed on voxel with highest signal intensity within locations anatomically	Y[m]	(Used participant data from Clewett et al., 2016.) Higher CR in older vs younger adults. LC-MRI contrast negatively correlated with

								consistent with LC.		high frequency-HRV (a measure reflecting cardiac parasympathetic influences). Mean CR(%): younger adults=15, older adults=18.
Matsuura 2013	Case-control	MCI/Dementia (PD, MSA)	PD, MSA, HC	41-92 (70)	64 (42)	3T	None reported.	High NM signal (ROI 2mm2). SI measured 3 times and averaged.	N	Reduced CR in MSA and PD vs HC, more prominent reduction in MSA. Mean CR(%): HC=15.0, PD=9.0, MSA=4.4
Miyoshi 2013	Case-control	MCI/Dementia (PD, AD)	PD, AD, HC	58-87 (72)	70 (61)	3T	None reported.	High NM signal (ROI 2mm2) in anterolateral area around 4th ventricle upper pons	Y [a]	Reduced CR in late PD vs HC, no significant difference between AD vs HC. Only graphical data presented. Median CR appears to be approx PD=1.025, AD=1.01, HC=1.05 $CR=SI_{LC}/SI_{PT}$
Mukai 2013	Case-control	MCI/Dementia (PD)	Idiopathic PD, POLG-1 associated parkinsonism, HC	52-89 (72)	40 (-)	3T	None reported	Highest NM signal (ROI 1mm2). Highest mean value of pixels in R+L LC per $1mm^2$ was averaged.	Y [b]	Reduced CR in idiopathic PD vs HC. Mean CR(%): idiopathic PD=5.4, HC=14.6
Ohtsuka 2013	Case-control	MCI/Dementia (PD)	Early and late PD, HC	50-80 (67)	83 (-)	3T	None reported.	High NM signal at slice through upper pons (1mm2 ROI). SI measured twice and averaged	Y [a]	Reduced CR in early and advanced PD vs HC but no significant difference between early and advanced PD. Median CR(%): HC=22.1, early PD=11.6, late PD=8.9
Ohtsuka 2014	Case-control	MC/Dementia (PD)	Early stage parkinsonism (early PD, MSA-P, PSPS), HC	47-80 (66)	75 (-)	3T	None reported.	High NM signal at slice through upper pons (1mm2 ROI). SI measured twice and averaged	Y [a]	Reduced CR in early PD than in other groups. Median CR(%):early PD=13.8, MSA-P=23.0, PSPS=24.3, HC=27.0

47

Study	Design	Condition	Groups	Age range (mean)	N (%F)	Field	Normalization	LC identification	Corr	Findings
Sasaki 2006	Case-control	MCI/Dementia (PD)	PD, HC	60-82 (70)	39 (56)	3T	The acquired images were correlated with macroscopic specimens at the level of midbrain and upper pons obtained from 2 cadavers (80 and 76 years old).	High NM signal in brainstem corresponding with LC location in gross specimens. SI measured 3 times and averaged.	Y[c]	Reduced CR in PD vs HC. Mean CR(%): HC=15.9, PD=8.17
Sasaki 2010	Case-control	Psychiatric disorder (MD, SZ)	MD, SZ, HC	21-83 (47)	69 (46)	3T	None reported.	High signal measured using 1mm2 cursor on semi-quantitative color map of LC section set as 30% of SI [PT]. SI measured 3 times and averaged.	N	Reduced CR in MD vs SZ and HC. Greater CR difference between SN-LC in SZ vs HC. Mean CR(%): HC=10.9, MD=7.3, SZ=9.8
Schwarz 2012	Case-control	MCI/Dementia (PD)	PD, HC	- (66)	22 (45)	3T	None reported.	ROI placed at high NM signal.	N	No difference in CR between PD and HC. Mean CR: PD=1.15, HC=1.13 $CR_{LC}=SI_{LC}/SI_{PT}$ (Data was pooled with 5 scans from a previous protocol with reduced voxel resolution (0.7x0.7mmx3mm)).
Schwarz 2016	Case-control	MCI/Dementia (PD)	PD, HC	41-87 (66)	69 (43)	3T	No report of image normalization within groups. Neuromelanin-related volumes from the 3 imaging protocols were normalized to one sequence that best matched the normative volumes from a recent histologic study.	Neuromelanin-related volumes for each imaging sequence calculated by including voxels above a signal intensity threshold (background signal + 3 s.d), then normalised to account for protocol-dependent effects.	N	Median LC volume reduction of 37% in PD vs HC. No correlation of LC volume loss with disease severity. Normalized mean LC volume = 16.7mm^3 (HC) and 11.7mm^3 (PD)
Shibata 2006	Cross-sectional	Age	HA	23-80 (50)	64 (56)	3T	None reported.	High NM signal in upper PT using 1mm2 cursor. SI in one slice measured 3 times and averaged.	N	Increased CR up to 40-59yrs which decreased in older adults. Mean CR(%): all ages=10.7, 20's=8.5, 30's=9.5, 40's=12.9, 50's=12.1, 60's=11.2, 70+=10.6. No significant difference

										between men=10.5 and women=11.1.
Shibata 2007	Case-control	Psychiatric disorder (MD)	MD, HC	22-83 (49)	63 (49)	3T	None reported.	High NM signal in PT. SI was measured in 3 contiguous sections, 3 times and averaged.	N	Reduced CR of rostral and middle LC in MD vs HC. No correlation with psychiatric rating scales. Mean CR(%):HC=11.9 (middle), 6.9 (rostral), 7.5 (caudal) Mean CR(%): MD=7.8 (middle), 5.2 (rostral), 6.7 (caudal)
Shibata 2008	Case-control	Psychiatric disorder (MD, SZ)	MD, SZ, HC	22-64 (44)	72 (44)	3T	None reported.	High NM signal in upper PT. SI in one slice measured 3 times and averaged.	N	Reduced CR in MD vs HC and SZ. Greater CR difference between SN-LC in SZ vs HC. No correlation with psychiatric rating scales. Mean CR(%):HC=11.0, SZ=10.0, MD=7.7
Takahashi 2015	Case-control	MCI/Dementia (AD)	AD, MCI, HC	59-87 (-)	95 (53)	3T	None reported.	ROI (1mm2) traced manually using peak NM signal around floor of 4th ventricle. Average SI from 3 measurements.	N	CR[LC] reduced in AD and MCI vs HC. No significant difference in CR between AD, MCIc and MCInc. Median CR(%): AD=9.3, MCIc=6.9, MCInc=7.7, HC=14.4
Watanabe 2014	Case-control	Psychiatric disorder (SZ)	SZ, HC	17-69 (35)	104 (48)	3T	None reported.	ROI traced manually around high NM signal. Average and maximum SI for ROI calculated. Average SI and area measured within ROI using 3 consecutive slices	N	No difference in CR or area between SZ and HC. Mean CR(%): SZ=14, HC=13 Mean area of LC (mm2): SZ=10.8, HC=11.4
Standard T1-weighted structural MRI										
Adhikarla 2016	Cross-sectional	Different kinetic models on 11[C]MENET PET image	HA	43-66 (54)	6 (0)	3T	Coregistration between PET and 3D T1 weighted MPRAGE image not described.	Neuroanatomical atlas by Haines and regions of focal uptake on the PET image were used to guide delineation.	Y[j]	The LC and other regions were found to exhibit norepinephrine transporter (NET) localisation.

49

		quantification								
Buysse 2004	Cross-sectional	Wakefulness	HA	25-49(37)	13 (77)	1.5T	Each subject's PET data was coregistered to their T1 weighted MRI image, spatially normalized into Talairach space and smoothed with a Gaussian kernel FWHM 10mm. Alignments and coregistration used a modification of Woods' automated algorithms for PET to PET and PET to MRI registration	Volume of interest analysis coordinates were determined a priori by the senior author, a neuroanatomist. Volumes of interest measured 10x10x8mm.	Y[j]	Evening wakefulness is associated with increased relative metabolism in brainstem. **Talairach** coordinates for volume midpoint of LC = R (10 -38 -20), L(-10 -38 -20). **Talairach** coordinates for maximally significant voxel for LC= R(6 -36 -24), L(-8 -34 -16)
Garcia-Lorenzo (II) 2013	Case-control	MCI/Dementia and sleep disorder(PD +/- RBD)	PD (+/- RBD), HC	18-75 (60)	55 (40)	3T	Voxel based analysis and voxel based diffusion imaging performed from 3D T1 weighted images	Voxel based diffusion imaging	Y[e]	Patients with RBD showed significant increases in fractional anisotropy in an area including the coeruleus/subcoeruleus (-11 -37 -30) cluster size 309mm^3
Germain 2007	Case-control	Psychiatric disorder (MD)	MD, HC	-(38)	25 (80)	1.5T	PET images coregistered to MRI images.	Volume of interest analysis using previously published coordinates (Buysse 2004: **Talairach** L(-10 -38 -20) R (10 -38 -20))	Y[j, k]	MD showed smaller increases in regional cerebral metabolic rate of glucose during evening relative to morning wakefulness in regions inc LC

Table 2. MRI parameters and outcome measures used by studies that reported data on the LC using neuromelanin-optimized T1-weighted MRI

Study	MRI sequence	Magnetization preparation (IR or MT)	TR / TE (ms)	Echo train length	FA (degrees)	Number of slices	Slice thickness, inter-slice gap (mm)	In-plane matrix dimensions	Voxel size (mm3)	FOV (pixels)	No. of averages	Acquisition time	Plane of acquisition	Reference region for normalization, LC region sampled	Measurements were reported to be blinded
Astafiev 2010	-	-	600/14	-	120	20	-,-	-	0.43×0.43x2.5	-	-	-	Axial	LC only	N
Castellanos 2015	RARE	-	600/15	2	-	11	2, 0.2	512x408	0.43x0.43x2	220x175	4	12min	Perpendicular to 4th ventricle floor	NM-MRI images were normalized to the mean background SI, then thresholded to extract the hyperintense signal in LC. Optimum threshold obtained using ROC curve	N
Chen 2014	2D GRE-MTC-200	MT (300°, 1.2 kHz off-resonance, 10 ms duration)	260/2.68	-	40	11	-,0	416x512	0.39×0.39×3	162x200	7	12min 39sec	-	Pons, LC	N
	2D GRE-MTC-300-PKC	MT (300°, 1.2 kHz off-resonance, 10 ms duration)	260/2.68	-	40	11	-,0	416x512		162x200	7	12min 39sec	-		
	2D RARE	-	600/12	2	-	11	-,0	416x512		162x200	6	12min 34 sec	-		
Clewett 2016	RARE	-	750/12	-	120	11	2.5, 3.5	-	0.43x0.43x2.5	220	1	1min 53sec	Axial	PT, bilateral LC at 7mm below section through inferior edge of inf. colliculus	Y
Ehrminger 2016	3D RARE	-	900/15	-	180	-	-,-	-	0.4x0.4x0.3	-	3	-	-	Rostral pons and mesencephalon, bilateral LC	Y

Garcia-Lorenzo 2013	2D RARE	-	900/15	-	180	-	-,-	-	0.4x0.4x3	-	3	-	Axial	Rostral pontomesencephalic area and LC	N
Isaias 2016	RARE	-	670/12	4	-	12	3,-	-	0.5x0.6x3	212x164	5	7min 40sec	OA perpendicular to 4th ventricle floor	PT, bilateral LC	N
Keren 2009	RARE	-	600/14	-	90	10	3, 0	512x320	0.4x0.4x3	220x175.31x30	-	11min	Axial perpendicular to the plane of brainstem	Peak LC signal on each axial slice	N
Keren 2015	RARE	IR (TI=325, 825, 1325ms)	3000/varied between 9.8-39.8	2	180	8	2, 0.5	128x128	In-plane voxel size=0.31mm	400x400	3	3hr 11min	Axial perpendicular to the rostral-caudal plane of brainstem	Peak LC signal on each axial slice	N
Langley 2016	2D-GRE with modified MT pulse	MT (300°, 1.2 kHz off-resonance, 10 ms duration)	354/3.1	-	40	15	-,0	412x512	0.39×0.39×3	162x200	7	17min 12sec	-	Cerebral peduncle, LC	N
Mather 2017	RARE	-	750/12	-	120	11	2.5, 3.5	-	0.43x0.43x2.5	220	1	1 min 53 sec	Axial	PT, bilateral LC at 7mm below section through inferior edge of inf. colliculus	Y
Matsuura 2013	RARE	-	550/11	4	-	12	2.5, 0	448x311	0.45x0.64x2.5	200	6	9min	OA perpendicular to 4th	PT, LC at 7mm below section through inferior edge of inf. colliculus	Y

													ventricle floor		
Miyoshi 2013	RARE	-	600/13	2	-	-	2.5, 1	512x512	-	220	-	12min	Axial parallel to anterior/posterior commissure line	PT, bilateral LC	N
Mukai 2013	RARE	-	600/12.2	2	-	11	2.5, 1	-	-	-	-	6min 27sec	OA perpendicular to 4th ventricle floor	PT, bilateral LC	N
Ohtsuka 2013	RARE	-	600/14	2	90	10	2.5,1	512x320	0.42x0.68x2.5	220	8	12min	OA perpendicular to 4th ventricle floor	PT, bilateral LC	Y
Ohtsuka 2014	RARE	-	600/14	2	90	10	2.5, 1	512x320	0.42x0.68x2.5	220	8	12min	OA perpendicular to 4th ventricle floor	PT, bilateral LC	Y
Sasaki 2006	RARE	-	600/14	2	-	-	2.5, 1	512x320	0.31x0.36x2.5	220	8	12min	-	PT, LC	Y
Sasaki 2010	RARE	-	600/14	2	-	10	2.5, 1	512x320	0.42x0.68x2.5	220	-	12min	OA perpendicular to 4th ventricle floor	PT, LC	N*
Schwarz 2016	T1 spectral presaturation inversion recovery pulse	IR (TI not reported)	688/9	-	-	21	2.5, 0.25	-	0.47x0.47x2.5	-	4	12min	Axial	PT, LC	N

53

	T1 'off-resonance' MT pulse	MT (parameters not reported)	904/9	-	-	12	2.5, 0.25	-	0.47x0.47x2.5	-	4	12min 34sec			
	T1 spin echo with 'off-resonance' MT pulse	MT (parameters not reported)	600/10	-	-	12	2.5, 0.3	-	0.38x0.38x0.3	-	3	9min 32sec			
Schwarz 2012	RARE with spectral presaturation inversion recovery pulse	IR (TI not reported)	688/9	-	-	21	2.5, -	-	0.47x0.47x2.5	-	4	12min	Axial	PT, LC	Y
Shibata 2006	RARE	-	600/14	2	-	-	2.5, 1	512x320	0.43x0.69x2.5	220	-	12min	OA perpendicular to 4th ventricle floor	PT, LC at slice 7mm below inferior edge of inf. colliculus	Y
Shibata 2007	RARE	-	600/14	2	-	10	2.5, 1	512x320	0.42x0.68x2.5	220	-	12min	OA perpendicular to 4th ventricle floor	PT, LC (middle, rostral and caudal portions)	Y
Shibata 2008	RARE	-	600/14	2	-	10	2.5, 1	512x320	0.42x0.68x2.5	220	-	12min	OA perpendicular to 4th ventricle floor	PT, LC at slice 7mm below inferior edge of inf. colliculus	Y
Takahashi 2015	RARE	-	600/14	2	90	10	2.5, 1	512x320	0.42x0.68x2	220	8	12min	OA perpendicular to 4th ventricle floor	PT, LC at slice 7mm below inferior edge of inf. colliculus	Y
Watanabe 2014	3D-spoiled GRASS	MT (parameters not	38.4/2.4	-	20	40	2, -	480x320	-	220	-	3min 25s	OA perpendicular to the	Pons, LC	Y

	with MT contrast	reported)										brainstem		

IR=inversion recovery, TI=inversion time, TR= repetition time, TE = effective echo time, FA=flip angle, FOV= field of view, RARE=rapid acquisition with refocused echoes, GRE=gradient echo, MT=magnetization transfer, SI = signal intensity, CR = contrast ratio, CNR=contrast to noise ratio, SD=standard deviation, RBD= rapid eye movement sleep behavior disorder, SZ=schizophrenia, MD=major depression, GAD= generalized anxiety disorder, PTSD=post traumatic stress disorder, MCI=mild cognitive impairment, MCIc=MCI converted to AD, MCInc=MCI not converted to AD, AD=Alzheimer disease, PD=Parkinson disease, MSA-P=multiple stage atrophy with predominant parkinsonism, PSPS= progressive supranuclear palsy syndrome, HR= heart rate variability, HC=healthy controls, HA=healthy adults, HYA= healthy younger adults, HOA=healthy older adults, IBS=irritable bowel syndrome, CRPS=complex regional pain syndrome, LC= locus coeruleus, PT=pontine tegmentum, SN=substantia nigra, NM=neuromelanin, OA=oblique axial, ICBM=Internaional consortium for Brain Mapping, REM=rapid eye movement, Y=yes, N=no, NA=not applicable, MNI=Montreal Neurological Institute, tVNS=transcutaneous electrical stimulation of the sensory auricular branch of the vagus nerve, VNS=vagus nerve stimulation, ANT-R=revised attention network test, CRF=corticotrophin releasing factor, rsFC=resting state functional connectivity, PFC=prefrontal cortex, dACC= dorsal anterior cingulate cortex, RTPJ=right temporoparietal junction, MPH=methylphenidate, POP=Preparing to overcome Prepotency, SUIT=spatially unbiased infratentorial template, AFNI=Analysis of Functional NeuroImages

* followed by observer confidence ratings for visual differentiation of anonymized colour maps
[a] = 123I-metaiodobenzylguanidine (MIBG) myocardial scintigraphy
[b] = muscle histology, genetic analysis
[c]= post mortem LC count and/or histological analysis
[d]=SPECT
[e]= overnight video and EMG
[f] = pulse rate and respiration depth
[g]= pupillometry
[h]= continuous polysomnographic and video recordings during scan
[i]=heart rate and salivary cortisol
[j]=Positron emission tomography
[k]=electroencephalogram
[l]=polysomnography and salivary melatonin
[m]= heart rate variability

Table 3: Studies that reported data on the LC using functional MRI

Study	Study design	Experimental manipulation	Population sampled	Age range (mean) in yrs	N (%F)	MRI magnet strength	Acquired voxel size (mm³)	Correction for cardiac and respiratory signals	Reported coregistration method	Identification of LC	Task used	Adjunctive non-MRI methods	Main LC findings and coordinates (x, y, z) (MNI unless stated otherwise)	Cognitive process
Event-related BOLD-FMRI studies														
Brooks 2017	Cross-sectional	Pain	HA	18-51 (25)	20 (50)	3T	1.5x1.5 x3.5	Y	Individual functional data was coregistered to the T1 structural scan using a combination of fieldmap based unwarping, boundary based registration and FLIRT. Functional data were smoothed with 3mm FWHM Gaussian kernel and high pass temporally filtered (120s).	A probabilistic template specific to the study group was generated and transformed into MNI space, then was used to define LC mask.	Thermal stimulation and RSVP attention task	Y[f]	Activation of LC during task (6 -36 -22) (4 -36 -24)	Top down
Gilam 2017	Case-control	Anger	Soldiers, civilians	-(20)	46 (0)	3T	-	N	Functional maps were manually co-registered to corresponding structural maps and they were incorporated into 3DI datasets through trilinear interpolation. The complete dataset was transformed into Talairach space and spatially smoothed with an isotropic 6 mm FWHM Gaussian kernel.	ROI was a cluster in brainstem which overlapped and reported to correspond with LC	Modified interpersonal anger-provoking Ultimatum Game played pre- and post-combat training (soldiers) or pre-/post-civil service (civilians).	N	Higher post-combat stress symptoms associated with higher activation increase in LC. **Talairach** LC (-7 -35 -18)	Bottom up
Hubbard 2011	RCT	Pain	IBS, HC	20-53 (36)	31 (100)	3T	-	N	An average of the first 10 realigned FMRI images for each subject was coregistered with their structural EPI image and then transformed into MNI space, 2mm³ isotropic voxels	Previously published templates (Keren 2009) to identify bilateral LC	Drug (CRF antagonist) or placebo in expectation of pain	N	IBS showed greater threat-induced LC activation during placebo vs HC. No drug	Bottom up

									and smoothed with 8mm Gaussian kernel.		paradigm		effects in IBS but reduced activation in HCL (-6 -36 -30)	
Kraus 2013	Cross-sectional	VNS	HA	20-37 (-)	16 (-)	1.5T	-	N	For group analysis of the brainstem activations all individual data were manually transformed to the anatomical brainstem dataset of one subject used as the reference brainstem. This was transformed into Talairach space and six prominent points on the brainstem defined as landmarks were used to complete linear alignment manually.	Contrast calculated between stimulation and sham conditions,activated areas compared to printed atlas (Kretschmann 1992)	tVNS	N	Greater BOLD activation in anterior stimulation vs sham **Talairach** (-6 -28 -24)	Bottom up
Krebs 2011	Cross-sectional	Novelty and reward	HA	-(25)	12 (58)	3T	1.5x1.5x2	Y (cardiac rate only)	T1 anatomical images were co-registered to SPM template and spatially normalized. Functional images were coregistered to the original T1 image, normalized and resliced to give 1x1x1mm3 voxel size, then smoothed with isotropic 3mm FWHM Gaussian kernel.	Activity clusters defined ROI (-8 -29 -21) for absence of reward	2x2 factorial design manipulating reward predictive value and novelty	N	Activation during familiar reward > familiar no reward in regions inc LC (-5 -32 -25)	Bottom up
Krebs 2013	Cross-sectional	Novelty	HA	19-28 (23)	18 (67)	3T	3x3x3	N	Anatomical images were spatially normalized with reference to SPM T1-template image. All functional EPIs were normalized based on the T1-derived normalization parameters, resliced to 2x2x2mm3 voxel size and smoothed with isotropic 6mm FWHM Gaussian kernel.	Individual ROIs were manually segmented on T2* anatomical scans	Picture-word interference task	N	Familiar incongruent trials associated with activation in regions inc. LC (-4 -34 -22)	Top down/motor
Krebs 2017	Cross-sectional	Unexpected events (novelty,	HA	18-39 (34)	21 (57)	3T	1.7x1.7x2	N	After coregistering all scans to the SPM T1 template image, the T1-MPRAGE anatomical scan was spatially normalized to the template (resliced to isotropic 1 mm voxels). The same	The LC was segmented manually based on the individual T1-TSE images using MRIcron. To test	Oddball task with face stimuli	N	Activation during task average LC ROI outer boundaries (-5 -41 -19) (-6 -38 -31)	Top down

57

		emotional conte nt)						parameters were used to coregister and normalize the T1-TSE image (resliced to isotropic 1 mm voxels). Functional EPIs were slice-time corrected, and spatially realigned to the first acquired EPI. Next, EPIs were normalized based on the T1-derived normalization parameters, resliced to isotropic 1.5 mm voxels, and smoothed with an isotropic FWHM Gaussian kernel of 3.5 mm. A manual co-registration check confirmed a good alignment of the brainstem in all anatomical and functional images within and across participants.	whether activity modulations in the LC are primarily related to generalized regional activity and/or unspecific physiological noise, they extracted BOLD parameter estimates (beta values) from spheres in two control regions.					
Laureiro-Martinez 2014	Cross-sectional	Decision-making	HA	-(34)	63 (17)	-	-	N	Not reported	Not reported.	Four-armed bandit task	N	Exploitation>exploration L LC (-4 -32 -14) (-8 -32 -26)	Top down
Liddell 2005	Cross-sectional	Fear	HA	-(32)	22 (50)	1.5T	-	N	Not described	Contrast calculated for fear vs neutral faces in ROI using brainstem mask	Brief presentation of facial signals of fear (unconscious detection)	N	Subliminal fear signals activate regions including LC (-2 -36 -23)	Bottom up
Meletti 2015	Cross-sectional	Cataplexy	HYA	8-16 (11)	21 (38)	3T	3x3x3	N	All functional images were normalized to the MNI template and smoothed with 8mm FWHM Gaussian kernel.	Whole brain GLM analysis	Watch a funny video to induce laughter +/- cataplexy	Y[h]	During cataplexy, activation of regions including LC L(-10 -28 -12) R(10 -28 -12)	Bottom up
Mohanty 2008	Cross-sectional	Attention, motivation	HA	-(27)	9 (44)	3T	3x3x3	N	Functional images were coregistered to the anatomical image using the EPI template in SPM2 to transform into MNI	Exploratory whole brain analysis	Spatial attention task in hungry and	N	Hunger selectively enhanced activity in	Bottom up

									space. Smoothed with an isotropic 7mm FWHM Gaussian kernel.		satiated states		regions including LC to food vs tool-related cues (9 -42 -30)	
Morey 2015	Case-control	Fear	PTSD, HC	-(42)	16 (24)	3T	3.75x3.75x3.75	N	Functional images for each subject were corrected for head motion and coregistered to that subject's anatomical image, spatially smoothed with Gaussian kernel 5mm FWHM.	8mm sphere ROI using prior localisation with NM-MRI (Astafiev 2010)	Preconditioning, fear conditioning and generalization	N	PTSD showed biased activation toward high-intensity stimuli in regions inc LC (0 -32 -8)	Bottom up
Murphy 2014	Cross-sectional	Attention (to vary pupil diameter)	HA	21-48 (29)	14 (43)	3T	3.5x3.5x3.5	Y	Functional images were normalized to the ICBM EPI template using the unified segmentation approach. Data was resliced to 2x2x2mm3 voxel resolution and smoothed with 6mm FWHM Gaussian kernel.	Previously published LC mask (Keren 2009) to identify ROI	Visual oddball task - an attentional paradigm with known effects on pupil diameter	Y [g]	LC covaried with pupil diameter: At rest (-4 -32 -30) During task with (2, -30 -22) and **without smoothing (0 -32- 20).** There was a stronger response to the target stimulus.	Top down
Napadow 2013	Cross-sectional	Nausea	HA	21-49 (27)	28 (100)	1.5T	-	N	Functional data was spatially normalized to MNI space using anatomical data and FNIRT.	Two approaches: a whole brain GLM approach and a percept-based approach where functional data was analysed relative to subjects' nausea ratings.	The nauseogenic stimulus was a standardized visual presentation of alternating black and white stripes with left-to-right circular motion	N	Phasic activity preceding nausea was found in brain regions including LC (-6 -38 -24)	Bottom up
Neufang	Cross-section	Attention	HA	-(25)	47 (49)	3T	-	N	Functional images were spatially normalized into MNI	ROIs defined by using the Wake	ANT to examine	N	Alerting condition	Top down

59

2015	al								space, resampled to 2x2x2mm3 voxel and smoothed with 8mm FWHM Gaussian kernel.	Forest University PICKATLAS	attentional functions - alerting, orienting and executive control		activated LC L(-4 -20 -2) R(2 -20 -2)	
Payzan-LeNestour 2013	Cross-sectional	Unexpected uncertainty (decision-making)	HA	-(23)	18 (50)	3T	3.5x3.5 x3.85	Y	Not reported.	Previously published LC mask (Keren 2009) to delineate LC	6-armed restless bandit decision task with fluctuations in unexpected uncertainty	N	Effect of unexpected uncertainty in regions including LC deactivation (-2 -37 -17)	Top down
Schilbach 2011	Cross-sectional	Action control	HA	21-37 (27)	23 (52)	3T	3.1x3.1 x3.1	N	EPI images were corrected for head motion. The mean realigned functional image for each subject was spatially normalized to the MNI single subject template using the 'unified segmentation' approach. Resampled to 2x2x2mm3 voxels and spatially smoothed using 8mm FWHM Gaussian kernel.	Functional activations localised using SPM anatomy toolbox/maximum probability map (Eickhoffet 2006)	Congruent and incongruent motor responses to social and nonsocial stimuli	N	Incongruent responses recruited LC L(-8 -28 -18) R(9 -27 -18)	Top down/ motor
Schmidt 2009	Cross-sectional	Attention	HA	-(25)	31 (55)	3T	3x3.4x3 .4	N	Functional images were normalized to the MNI EPI template, spatially smoothed using 8mm FWHM Gaussian kernel.	LC reference coordinates derived from Liddell 2005 and Sterpenich 2006 to obtain small spherical volumes 8mm radius around ROI for LC	Psychomotor or vigilance task (to measure sustained attention)	Y[l]	Maintaining attention in the evening was associated with higher activity in evening than morning chronotypes in LC R (4 -32 -18) R (4 -26 -24)	Top down
Schulte 2016	Cross-sectional	Pain	HA	-(29)	21 (62)	3T	1.25x1. 25x2.5	Y	T1 structural image for each subject was coregistered to the mean functional image of the same person then normalized using an iterative segmentation-	Previously published coordinates of LC (Keren 2009) used as a priori	Nociceptive ammonia stimulation of L nasal mucosa	N	Trigeminal nociceptive stimulation activated regions	Bottom up

60

									normalization approach. The normalization parameters were applied to the functional images and these were upsampled to 1x1x1mm3 voxels and smoothed using 4mm FWHM isotropic Gaussian kernel. Images were corrected for physiological noise.	ROI (6 mm spheres)			including LC (8 -39 -33)	
Sclocco 2016	Cross-sectional	Pain	HA	-(33)	11 (27)	7T	1.2x1.2 x1.2	Y	The T1 anatomical data was coregistered to the ICBM152 MNI template. The transform matrices were inverted and applied to a brainstem mask originally defined in ICBM152 space (Beissner et al.,2013), and this mask was transformed to the individual functional space.	GLM exploratory analysis.	Inflated pressure cuff over lower left leg to induce sustained pain, or resting condition	Y[f]	Pain>rest LC activation R (5, -36, -30)	Botto m up
Sterpe nich 2006	Cross-sectional	Emoti onal memo ry	HA	-(22)	30 (53)	3T	3.4x3.4 x3.4	N	Functional images were normalized to the MNI EPI template, spatially smoothed using 8mm FWHM Gaussian kernel	LC coordinates derived from Liddell 2005 to obtain small spherical volumes 10mm radius around ROI for LC	Forced choice (yes/no) recognition task for neutral faces on background of negative or neutral images	Y[g]	The LC responds significantly during the successful recognition of neutral events encoded in an emotional context. LC and amygdala are more functionally connected during correct recognition in emotional vs neutral context R(2 -32 -20), R(6 -36 -24) R(6 -34 -28)	Top down
Steuw e 2014	Case-control	Direct gaze proce ssing	PTSD, HC	-(32)	32 (100)	3T	2x2x2	N	Not described.	Previously published coordinates (-2 -36 -23) served	Virtual reality paradigm involving	N	PTSD showed increased activation in regions	Botto m up

		(threat)								as origin for 10mm radius spherical ROI (Liddell 2005)	faces with direct vs averted gaze		including LC during direct gaze (-2 -32 -22)	
Vande walle 2007	Cross-sectional	Light	HA	19-27 (-)	15 (53)	3T	3.4x3.4 x3	N	Functional scans were spatially normalized to EPI template conforming to MNI space and spatially smoothed with 8mm FWHM Gaussian kernel.	Previously published coordinates of LC (Sterpenich 2006) used as a priori location for spherical volumes (10mm radius) for analysis	Exposure to monochromatic violet, blue or green light while performing working memory task	N	Blue light activated regions including LC L(-6 -38 -20) R(6 -30 -16)	Botto m up
Von der Gable ntz 2015	Cross-sectional	Task-switch ing (cogni tive contro l)	HA	20-26 (23)	16 (44)	1.5T	3.125x3 .125x5	N	Functional (EPI), T1 structural and inversion-recovery echo planar (IR-EPI) scans were obtained. EPIs were coregistered to the IR-EPI, the T1 scan was coregistered to the IR-EPI and segmented,then the transformation matrix from the segmentation step was applied to the EPIs. Resampled to 2x2x2mm3 voxels and smoothed using 8mm FWHM Gaussian kernel.	Contrast of switch feedback vs correct feedback	Modified Eriksen–Flanker task: participants derived the correct stimulus–response association based on a feedback given after each flanker stimulus	N	Switch signal associated with activity in brain regions inc LC R (10 -32 -14)	Top down
Xuan 2016	Cross-sectional	Attent ion	HA	18-49 (26)	24 (46)	3T	3.75x3. 75x4	N	Brainstem images were coregistered to the MNI ICBM152 template: a mask of MNI-152 brainstem was created across axial section z=13 to z=-57. Voxels inside the mask set to 1, others set to 0. Global coregistration of EPI images to MNI ICBM152 space was completed based on normalization parameters of mean EPI and resampled to 2x2x2mm2 voxels. Then, normalized EPIs were	LC location was referenced to previous studies (Minzenberg 2008, Keren 2009)	ANT-R to examine attentional functions - alerting, orienting and executive control	N	Alerting function activated regions including LC (2 -34 -20)	Top down

									coregistered to both MNI ICBM152 EPI template and the EPI template weighted by the brainstem mask. Images were spatially smoothed 8mm FWHM Gaussian kernel.					

Event-related BOLD and functional connectivity fMRI

Kohler 2016	Cross-sectional	Cognitive control	HA	18-56 (28)	45 (57)	3T	2.67x2.67x2.7	N	The functional images were corrected for differences in time acquisition. The coregistered structural images were segmented using the tissue probability maps of the ICBM template. Functional images were then spatially normalized to the MNI space using spatial normalization parameters estimated during the segmentation process. Smoothed with 6mm FWHM Gaussian kernel and high-pass filtered with a cutoff period of 128s. To improve the normalization procedure and verify brainstem results at the whole-brain level, data were normalized to the spatially unbiased infratentorial template (SUIT).	Contrast for incongruent vs congruent Stroop conditions. ROI analysis in brainstem using a mask image created by WFU Pickatlas. Data was normalised using SUIT toolbox	Manual Stroop color-word task to measure cognitive (inhibitory) control	N	Functional activation and connectivity patterns in LC are modulated by different demands of cognitive control. Activation for incongruent Stroop condition L LC (-6, -28,-13,) R LC (8, -28,-15). **Using SUIT L LC (-2, -32, -23) and R LC (6, -28, -21).** Distinct FC between LC and PFC, dACC, parietal and occipital regions.	Top down
Minzenberg 2008	RCT	Psychotropic medication (modafinil), cognitive control	HA	18-50 (33)	21 (43)	3T	3.4x3.4x3.4	N	Functional images were realigned to the first retained image in the block, adjusted for acquisition time then spatially normalized directly to the EPI template from the SPM library, via 6 parameter rigid body affine transformation. Images resliced to 2x2x2 and smoothed with 8mm FWHM Gaussian kernel.	LC defined as pontine cluster showing significant deactivation in task-independent drug effect	POP task requires cognitive control to overcome prepotent response	N	Modafinil was associated with decreased, task-independent tonic LC activity, increased task-related LC and PFC activity and increased	Top down

Study	Design	Domain	Group	Age	N (%)	Field	Voxel	Physio	Preprocessing	Analysis	Task		Results	Direction
													LC-PFC functional connectivity. Drug<placebo: R LC (12, -26, -17) (8, -30, -9), L LC (-10, -26, -12), Drug>placebo: R LC (8, -40, -15), (8, -16, -14), L LC (-4, -35, -12)	
Raizada 2007	Cross-sectional	Attention	HA	-(26)	12 (75)	3T	-	N	Preprocessing included slice timing correction, motion correction and normalization to the MI1305 stereotactic space (3mm cubic voxels). Smoothed with 8mm Gaussian kernel.	Task-difficulty weighted contrast yielded brainstem and frontal ROIs	Audiovisual task in which trial difficulty and onset times varied unpredictably	N	Brainstem responded to most difficult trials showing phasic pattern, consistent with LC (0 -33 -24)	Top down
Functional connectivity studies														
Anticevic 2014	Case-control	Psychiatric disorder (SZ)	SZ, HC	-(27)	165 (54)	3T	-	N	Structural image was transformed to **Talairach** space and functional images were coregistered to the structural image with 3x3x3mm3 resampling.	Amygdala seed based, whole brain rsFC	Resting state	N	SZ high risk group had increased amygdala rsFC with LC **Talairach** (2 -40 -26)	NA
Bar 2016	Cross-sectional	-	HA	20-57 (29)	154 (53)	3T	2.5x2.5 x2.5	Y (respiratory signal only)	To improve the normalization procedure within the brainstem, neuroimaging data were normalized to the spatially unbiased infratentorial template (SUIT). No smoothing. Data was corrected for physiological noise by applying the RETROICOR approach. For the whole brain data, a within-subject registration was performed between structural	Seed region LC to whole brain. LC was identified using anatomical atlas of the human brainstem (Naidich 2009).	Resting state	N	LC is functionally integrated into the executive-control network R (7, -34, -21) L (-5, -34, -21)	NA

64

Study	Design	Condition	Group	Age	N (%)	Field	Voxel		Preprocessing	Seed/ROI	Task		Results	
									and functional images. The coregistered anatomical images were segmented and functional images were normalized to MNI space using the deformation field created during the segmentation process. Smoothed with 6mm FWHM Gaussian kernel.					
Erpeld ing 2014	Case-control	Pain (CRP S)	CRPS, HC	10-17(14)	24 (18)	3T	3x3x3	N	Functional scans were coregistered to anatomical scans using FLIRT and nonlinearly registered to MNI space using FNIRT. No smoothing.	Medial and lateral habenula seed based whole brain rsFC	Resting state	N	CPRS showed lateral habenula rsFC to regions including LC (-14 -34 -28)	NA
Henck ens 2012	RCT	Stres s	HA	19-28 (-)	48 (0)	1.5T	-	Y	All realigned functional images were coregistered with the T1 structural image using normalized mutual information maximization. The anatomical image was subsequently used to normalize all scans into MNI space. Functional images were resampled to 2mm isotropic voxels. Smoothed with 8mm FWHM Gaussian kernel.	Amygdala seed, LC ROI defined using 5mm radius sphere around coordinates from previously published study (Astafiev 2010)	Resting state hydrocortis one vs placebo	N	Hydrocortisone reduced rsFC of amygdala with LC (-8 -36 -22)	NA
Kahnt 2013	Cross-section al	Decisi on makin g	HA	-(22)	21 (57)	3T	2.75x2. 75x3	N	Not reported.	RTPJ seed region with LC ROI, verified anatomically using coordinates from published study (Keren 2009)	Value-based choice task during scanning	N	Elemental salience-dependent change in functional connectivity between RTPJ and LC (-6 -37 -23)	NA
Kline 2016	Case-control	Psych otropi c medic ation (MPH)	HA	19-31 (-)	48 (67)	3T	-	N	A mean functional image was constructed from the realigned image volumes for each subject. The structural image was coregistered with these mean images and segmented for normalization with affine registration followed by	LC seed region to whole brain. LC coordinates derived from template (Keren 2009) L(-5 -37 -26) R(5 -37 -26)	Resting state	N	Positive rsFC with cerebellum in both groups, less positive rsFC in MPH. MPH showed significant positive rsFC	NA

									nonlinear transformation. The normalization parameters determined for the structural volume were then applied to the corresponding functional image volumes for each subject. Smoothed with 8mm FWHM Gaussian kernel.				with R hippocampus.	
Lerner 2009	Cross-sectional	Emotionality	HA	25-41 (-)	26 (19)	3T	-	N	The functional images were superimposed on 2D anatomical images and incorporated into the 3D data sets through trilinear interpolation. The complete data set was transformed into **Talairach** space.	Amygdala seed to whole brain, negative vs neutral music contrast used to define volumes of interest for LC in each subject.	Music clips of negative and neutral emotional values, during eyes open/closed /viewing video	N	Amygdala significantly co-activated with LC when closing eyes in the presence of negative music **Talairach coordinates** R LC(4, -36, -34), (2, -38, -24), (2, -26, -46), (4, -30, -30), (5, -16, -12), (2, -40, -36), (4, -32, -30), (0, -36, -44), (4, -18, -18), (9, -9, -27). L LC (-4, -34, -30), (-6, -34, -16), (-12, -9,-27)	NA
Meeten 2016	Case-control	Psychiatric disorder (GAD)	GAD, HC	-(29)	40 (88)	1.5T	3x3x3	Y (cardiac signal only)	Normalization to the EPI template in standard MNI space, smoothing with 8mm FWHM Gaussian kernel. Data was further filtered regressing against the realignment parameters, and the signal averaged over whole brain voxels. All images were filtered by band pass filter (0.01-0.08Hz) to reduce effect of high frequency physiological noise.	Amygdala seed region to whole brain	Four 5min resting state periods followed by 6min easy visuomotor tracking task. After 2nd/3rd resting block participants underwent an induction	Y[m]	Positive correlation between anxiety score and pre- to post-induction changes to FC between R amygdala and LC (-8, -28, -18)	NA

											procedure designed to elicit worrisome thoughts.			
Metzger 2015	RCT	Psychotropic medication	HA	20-32 (24)	19 (0)	3T	3x3x3.75	N	Functional images were spatially normalized to MNI template and smoothed with 8mm FWHM Gaussian kernel.	L LC seed region (-4 -30 -18) 3mm radius sphere, whole brain rsFC. Not mentioned where coordinates were obtained from.	Resting state	N	Treatment with reboxetine altered rsFC of LC, i.e. increased rsFC with amygdala, thalamus, tectum.	NA
Moulton 2014	Case-control	Migraine	Migraine patients, HC	-(32)	24 (71)	3T	3.5x3.5x4	N	All functional volumes were motion corrected, mean-based intensity normalized by the same factor and smoothed with a 5mm FWHM filter, and a 150s high pass temporal filter applied. Functional images were then coregistered with anatomical images using FLIRT, an automated affine registration algorithm.	Hypothalamus seed based, whole brain rsFC	Resting state	N	Migraineurs showed enhanced rsFC in hypothalamus to regions including LC (8 -34 -26)	NA
Steuwe 2015	Case-control	Direct gaze processing (threat)	PTSD, HC	-(32)	32 (100)	3T	2x2x2	N	Not reported.	LC seed region (2, -32 -22) to whole brain. LC defined as 5mm sphere around coordinates derived from previous results (Steuwe 2014)	Virtual reality paradigm involving direct vs averted gaze	N	PTSD showed increased LC rsFC to frontal, limbic and subcortical areas. Positive correlation between rsFC to parahippocampal gyrus and PTSD symptom severity.	NA
Van Marle 2010	Case-control	Stress	HA	18-25 (21)	26 (100)	3T	-	N	Mean functional volume was coregistered to the structural image, then images were transformed into MNI space and resampled into 2mm isotropic voxels. Smoothed with	Amygdala seed region, LC as ROI using 10mm radius sphere around previously	Stress condition induced by showing short movie clip of	Y[i]	Post-stress enhanced rsFC of amygdala and LC (4 -24 -18)	NA

67

									8mm FHWM Gaussian kernel.	reported coordinate (Schmidt 2009)	extreme violence in scanner, then resting state scan			
Zhang 2016	Cross-section al	-	HA	18-49 (-)	250 (58)	3T	-	Y (by accou nting for physio logical noise in anothe r sampl e)	A mean functional image volume was constructed for each subject per run and coregistered with the structural image. Then segmented for normalization with affine registration and nonlinear transformation. The normalization parameters for the structural image were applied to the corresponding functional volume for each subject. Smoothed with 8mm FWHM Gaussian kernel.	LC seed region (5 -37 -20) obtained from peak coordinates from Keren 2009, whole brain rsFC	Resting state	N	LC showed widespread rsFC to other regions. rsFC with fronto-parietal cortex and cerebellum increases with, rsFC to visual cortex decreases with age	NA

IR=inversion recovery, TI=inversion time, TR= repetition time, TE = effective echo time, FA=flip angle, FOV= field of view, RARE=rapid acquisition with refocused echoes, GRE=gradient echo, MT=magnetization transfer, SI = signal intensity, CR = contrast ratio, CNR=contrast to noise ratio, SD=standard deviation, RBD= rapid eye movement sleep behavior disorder, SZ=schizophrenia, MD=major depression, GAD= generalized anxiety disorder, PTSD=post traumatic stress disorder, MCI=mild cognitive impairment, MCIc=MCI converted to AD, MCInc=MCI not converted to AD, AD=Alzheimer disease, PD=Parkinson disease, MSA-P=multiple stage atrophy with predominant parkinsonism, PSPS= progressive supranuclear palsy syndrome, HR= heart rate variability, HC=healthy controls, HA=healthy adults, HYA= healthy younger adults, HOA=healthy older adults, IBS=irritable bowel syndrome, CRPS=complex regional pain syndrome, LC= locus coeruleus, PT=pontine tegmentum, SN=substantia nigra, NM=neuromelanin, OA=oblique axial, ICBM=Internaional consortium for Brain Mapping, REM=rapid eye movement, Y=yes, N=no, NA=not applicable, MNI=Montreal Neurological Institute, tVNS=transcutaneous electrical stimulation of the sensory auricular branch of the vagus nerve, VNS=vagus nerve stimulation, ANT-R=revised attention network test, CRF=corticotrophin releasing factor, rsFC=resting state functional connectivity, PFC=prefrontal cortex, dACC= dorsal anterior cingulate cortex, RTPJ=right temporoparietal junction, MPH=methylphenidate, POP=Preparing to overcome Prepotency, SUIT=spatially unbiased infratentorial template, AFNI=Analysis of Functional NeuroImages

* followed by observer confidence ratings for visual differentiation of anonymized colour maps
[a] = 123I-metaiodobenzylguanidine (MIBG) myocardial scintigraphy
[b] = muscle histology, genetic analysis
[c]= post mortem LC count and/or histological analysis
[d]=SPECT
[e]= overnight video and EMG
[f] = pulse rate and respiration depth
[g]= pupillometry
[h]= continuous polysomnographic and video recordings during scan
[i]=heart rate and salivary cortisol
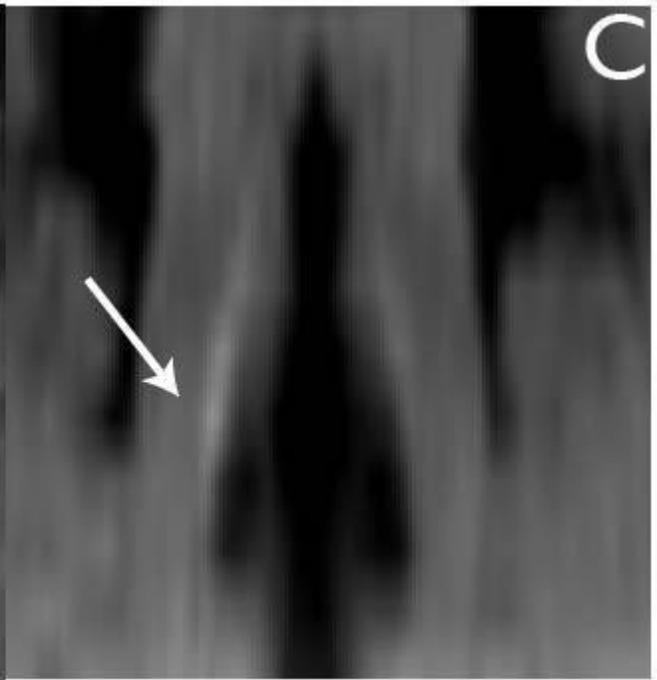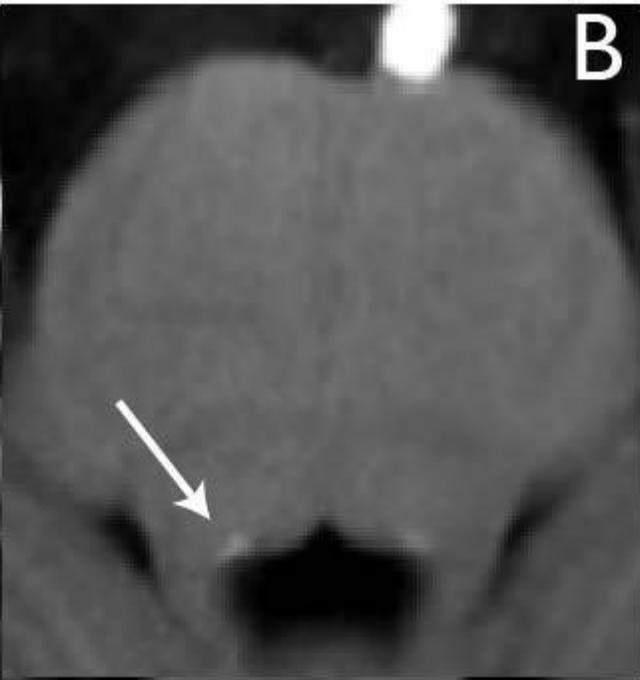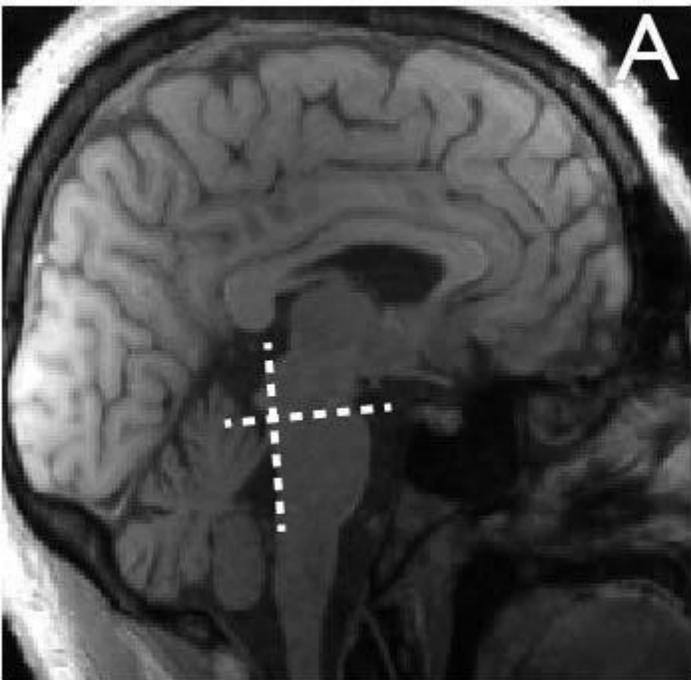[j]=Positron emission tomography
[k]=electroencephalogram

[l]=polysomnography and salivary melatonin
[m]= heart rate variability

Table 4: Summary of recommendations for future studies

Structural MRI studies	*Functional MRI studies*
● Calculate LC-CR using the formula adopted in this review (Eq.1) to allow comparison of findings and greater statistical power in future meta-analyses. ● Investigate LC integrity in clinical groups such as AD patients, and try to measure CR and LC volume. ● Explore the potential to increase sensitivity and specificity to age-related changes and neurodegenerative conditions by assessing CR across the rostro-caudal extent of LC, using thinner MRI slices and comparing imaging data to existing disease biomarkers. ● Normalize LC signal intensity to that of a reference region, and investigate the importance of correcting results for participant age, smoking status, reference region (pontine) signal intensity variability and partial volume effects.	● Investigate the factors contributing towards location coordinate distribution including variation in coregistration methods and differences in LC position across individuals. ● Use the highest possible fMRI resolution. Coregister functional images with structural LC templates generated from the study sample and report the method and precision of coregistration in detail. Previously published template maps may help to assess the accuracy of the LC-ROI obtained. ● Perform coregistration with specialized templates and spatial smoothing with appropriate justification. Correct functional BOLD data for cardiac and respiratory signals as well as head motion. ● Explore task designs and stimuli that trigger LC activation to investigate common mechanisms underlying LC activation, and study the potential of indirect measures of LC activity (HRV and pupillometry).